

ASYMPTOTIC ANALYSIS OF A SILICON FURNACE MODEL *

BENJAMIN M. SLOMAN[†], COLIN P. PLEASE[†], AND ROBERT A. VAN GORDER[†]

Abstract. Silicon is produced from quartz rock in electrode-heated furnaces by using carbon as a reduction agent. We perform an asymptotic analysis of a heat and mass transfer model of an experimental pilot furnace in order to determine the dominant chemical and thermal behaviour of the system. First, by prescribing a steady state temperature profile in the furnace we explore the leading order reactions in different spatial regions, as well as early time behaviour. We are able to obtain asymptotic solutions which compare well with numerical simulations. Utilising the dominant balances found when the temperature is prescribed, we next reduce the full model to two coupled partial differential equations for the time-variable temperature profile within the furnace and the concentration of solid quartz. These equations account for diffusion, an endothermic reaction, and the external heating input to the system. A moving boundary is found and the behaviour on either side of this boundary explored in the asymptotic limit of small diffusion. We note how the simplifications derived may be useful for future models and industrial furnace operation, and comment on insights from the model about furnace crust formation.

Key word. heat and mass transfer, silicon furnace, endothermic reaction, asymptotic analysis, multiple scales, moving boundary problems.

AMS subject classifications. 80A20, 92E20, 80M35, 35R37

1. Introduction. Silicon is an important material, being used in crystal form for semiconductors in solar panels and computers, as polysilicon in such things as paint and textiles, and as part of metallic alloys [18]. It is produced from the raw material quartz (SiO_2), using carbon as a reduction agent, in large furnaces which are heated by electrodes [2, 11, 18, 22]. In the furnaces numerous chemical reactions occur, as well as different types of interactions between solid, liquid, and gaseous phases. The high temperatures found (around 2000 K) are influenced by the chemical reactions and the electrical heating. Mathematical modelling is crucial to understand the interdependence between the physical and chemical effects taking place. In furnace operation a crust emerges, comprised of solid and viscous liquid substances, preventing raw material from reaching the hotter, lower part of the furnace and hence inhibiting the necessary reactions from taking place. To counter this the furnace is ‘stoked’ on an hourly basis, whereby the crust is manually broken up. This is a tedious operation, and thus it is of particular interest to see if this crust formation can be understood better. In [21] we produced a continuum model of a silicon furnace, simplifying the geometry to replicate a pilot furnace experiment. Here we build on this work by examining asymptotic limits of this model, in order to capture and better understand the underlying behaviour.

There is a wealth of mathematical literature on problems of coupled chemical and thermal effects. In [4, 13, 16] the authors consider catalytic converters and combustion. Here an exothermic reaction heats the system, causing an initial light-off behaviour [16] and the mechanisms by which the reaction switches off [4] are studied by asymptotic means. A separate, but linked, body of work examines competing exothermic and endothermic reactions [7, 17, 20, 24]. If there is just a single exothermic reaction, or two exothermic reactions, travelling wave solutions exist. However, the presence of the endothermic reaction, removing heat from the system, means these travelling waves can only exist for certain regions of the parameter space. In [3] premixed flames are considered and in [1] a model of coupled heat transfer and an endothermic reaction is analysed. Useful analogues of the behaviour in the model of Sloman et al. [21] can be found in work set in different physical contexts. In [5] the authors find a moving drying front in the roasting of a coffee bean, which separates a dry region from a pre-heating region. The behaviour of this narrow transition region is analysed using asymptotic methods. The processing of glass in a furnace is considered in [6], where a melted upper region and an unmelted lower batch region are separated by a downwards moving travelling front. In the context of tumour cells the authors of [12] find new discontinuous travelling waves for different hyperbolic PDE models. Although many chemical processes contain numerous reactions, it is possible to reduce the number of equations in mathematical models describing these processes by making certain simplifications. One of these is the quasi-steady state assumption [19], or pseudo-steady state hypothesis. There is a separation of timescales, so that after the initial fast timescale some of the variables can be

*This publication is based on work supported by the EPSRC center for Doctoral Training in Industrially Focused Mathematical Modelling (EP/L015803/1)

[†]Mathematical Institute, University of Oxford, Andrew Wiles Building, Radcliffe Observatory Quarter, Woodstock Road, Oxford, OX2 6GG, United Kingdom (Robert.VanGorder@maths.ox.ac.uk)

48 assumed to be in steady state, reducing the number of equations to be solved to find the other variables,
49 which vary over a longer timescale.

50 In Section 2 we present a summary of the model for a silicon furnace developed in [21], listing equations in
51 dimensional variables and giving brief descriptions of what these represent physically. We non-dimensionalise
52 this model in such a way as to ensure all dimensionless variables are order one in size, while parameters are
53 also order one, except for two which are small. In Section 3 we examine this model with the simplification
54 of a prescribed steady-state temperature profile in the limit of these small parameters going to zero. This
55 corresponds physically to the reaction between liquid quartz and carbon being instantaneous when compared
56 to the melting of solid quartz, and gas advection being instantaneous when compared to both these effects.
57 Using a prescribed temperature profile makes the leading order system of equations easier to solve and allows
58 us to capture the behaviour of the dominant chemical effects. We find that two spatial regions emerge, being
59 a lower, hot region where gas is produced from the solid carbon and quartz, and a cold, upper region where
60 SiO gas reacts with carbon particles and also condenses. We also find two timescales, with an initial fast
61 transience followed by a slower outer timescale. In Section 4 we consider asymptotics of the full problem,
62 where the varying temperature is coupled with chemistry and gas transport. We find that the leading order
63 problem comprises of an endothermic chemical reaction acting as a sink in the heat equation, which has
64 an external source. This differs from much of the literature discussed, which largely deals with exothermic
65 reactions (e.g. [4, 13, 16]). We find similar spatial regions to those which arise in Section 3 with a prescribed
66 temperature profile, with the difference that the spatial interface rises in the furnace with a travelling wave
67 type behaviour. We are particularly interested in both crust formation and the interface between the charge
68 and the gas cavity, given in this model by isotherm where quartz begins to melt. There is discussion of
69 the melting isotherm throughout Sections 3 and 4, and in Section 5 we give insights into crust formation.
70 Concluding remarks are given in Section 6.

71 **2. The Model.** We take the model for a silicon furnace from [21]. This is a continuum model for the
72 dynamics of chemical concentrations, gas partial pressures, material transport, and temperature within a
73 vertical section of a furnace. The model is applied to pilot furnace experiments, discussed in [21], and so
74 electrical effects are not considered. Heat transfers due to gas advection, conduction, radiation, exothermic
75 and endothermic reaction heat release or absorption, and an external energy source. Diffusion of gases is
76 neglected due to the high Péclet number (around 10^3), and for simplicity solids and liquids move in a constant
77 bulk flow. We give a summary of the model here, but further details are found in [21].

78 The model assumes that at any point in the furnace there is a mixture of one of seven chemical species.
79 These are three solid species: carbon - C, silicon carbide - SiC, and quartz - SiO₂(s); two liquid species:
80 ‘sticky’ quartz - SiO₂(l), and silicon - Si; and two gaseous species: carbon monoxide - CO, and silicon
81 monoxide - SiO. The model considers the effective concentration of these chemicals, denoted C_X [mol/m³]
82 for each species X. This gives the number of moles of X per unit volume of the mixture of all species in
83 the furnace. All the solids, liquids, and gases are considered to be locally at the same varying temperature
84 T [K], and there are assumed to be no voids in the furnace, so that any arbitrary volume is filled with a
85 combination of the chemical species modelled. The total gas pressure P_{TOT} is assumed to be constant, at 1
86 bar, created by the partial pressure of silicon monoxide, denoted P , and carbon monoxide. Both gases are
87 allowed to move at the same varying velocity $\mathbf{V}_g = U_g \mathbf{k}$. Advection of gases dominates over diffusion, so gas
88 diffusion is not included in the model. The imposition of constant total pressure and a no voids conditions
89 means that gas moves in order to equilibrate pressure. If gas is produced through reactions in one part of the
90 furnace, then it will move away from that region to keep the total pressure steady. Thus the gas velocity is
91 not explicitly stated, but is determined implicitly as part of the model. The solids and liquids are assumed to
92 move at a constant velocity $\mathbf{V}_s = -U_s \mathbf{k}$. We apply our model to the pilot furnace experiments, described in
93 [21], and so take U_s to be zero since material is not fed in to the furnace top during the experiments. As can
94 be seen in Figure 1, the prevailing structure in the pilot furnace is uni-dimensional. We are interested in the
95 location of crust formation, and this can be captured using a single spatial co-ordinate z , representing height
96 in the furnace. Although the gas cavity and the crater are distinct regions in experimental and industrial
97 furnaces, since we have a mixture of solids, liquids, and gases at all heights these regions are combined in
98 our model, with the joint region referred to as the base of the furnace.

99 The following chemical reactions are considered to take place in the furnace, with bracketed notation (s)
100 denoting a solid, (l) a liquid, and (g) a gas.

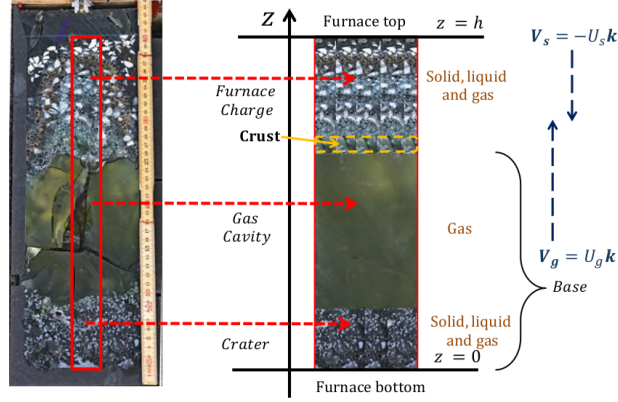


Fig. 1: The red box in the left hand image shows a typical vertical section in the pilot furnace. The horizontal variations are smoothed out in the right hand image to illustrate the approximation of the furnace geometry with a 1-D model. Reproduced from [21].



107 Using the relations $C_{\text{CO}} + C_{\text{SiO}} = C_g$, $C_{\text{CO}} = C_g(P_{\text{TOT}} - P)$, and $C_{\text{SiO}} = C_g P$, the dimensional model
 108 equations are

$$109 \quad (6) \quad \frac{\partial}{\partial t} \begin{pmatrix} C_{\text{C}} \\ C_{\text{SiC}} \\ C_{\text{SiO}_2(\text{s})} \\ C_{\text{SiO}_2(\text{l})} \\ C_{\text{Si}} \\ C_g(P_{\text{TOT}} - P) \\ C_g P \end{pmatrix} + \frac{\partial}{\partial z} \begin{pmatrix} -U_s C_{\text{C}} \\ -U_s C_{\text{SiC}} \\ -U_s C_{\text{SiO}_2(\text{s})} \\ -U_s C_{\text{SiO}_2(\text{l})} \\ -U_s C_{\text{Si}} \\ U_g C_g(P_{\text{TOT}} - P) \\ U_g C_g P \end{pmatrix} = \begin{pmatrix} -2 & 0 & 0 & 0 & 0 & -1 \\ 1 & 0 & 0 & 0 & -1 & 0 \\ 0 & 0 & 0 & -1 & 0 & 0 \\ 0 & 1 & -1 & 1 & 0 & -1 \\ 0 & 1 & -1 & 0 & 2 & 0 \\ 1 & 0 & 0 & 0 & 1 & 1 \\ -1 & -2 & 2 & 0 & -1 & 1 \end{pmatrix} \begin{pmatrix} R_1 \\ R_2 \\ R_3 \\ R_{-2} \\ R_4 \\ R_5 \end{pmatrix},$$

110

$$111 \quad (7) \quad \frac{RT C_g}{P_{\text{TOT}}} + \sum_{\text{solids and liquids } i} C_i \frac{M_i}{\rho_i} = 1,$$

112

$$113 \quad (8) \quad \begin{aligned} & \frac{\partial}{\partial t} (T(A_f(\sigma_s + \sigma_g) + A_{gr}\sigma_{gr})) + \frac{\partial}{\partial z} (T A_f(-U_s \sigma_s + U_g \sigma_g)) \\ & = \frac{\partial}{\partial z} \left((A_f k_f + A_{gr} k_{gr}) \frac{\partial T}{\partial z} + A_f \beta T^3 \frac{\partial T}{\partial z} \right) + A_f \sum_j dH_j R_j + (A_f + A_{gr}) F, \end{aligned}$$

114 where

$$115 \quad (9) \quad \begin{pmatrix} R_1 \\ R_2 \\ R_{-2} \\ R_3 \\ R_4 \\ R_5 \end{pmatrix} = \begin{pmatrix} k_1 r_C C_C (P - P_1(T))^+ \\ k_2 (P - P_2(T))^+ \\ k_{-2} C_{\text{SiO}_2(l)} C_{\text{Si}} \\ k_3 C_{\text{SiO}_2(s)} (T - T_M)^+ \\ k_4 C_{\text{SiC}} (P - P_4(T))^+ \\ k_5 C_{\text{SiO}_2(l)} C_C \end{pmatrix}.$$

116 Here we have denoted $R = 8.314 \text{ J/molK}$ as the gas constant, M_i the molar mass of each species, and
 117 ρ_i the corresponding species density, assumed to be constant for solids and liquids. A_f and A_{gr} are the
 118 cross-sectional surface areas of the pilot furnace and graphite crucible, respectively, σ_s , σ_g , and σ_{gr} are
 119 the heat capacities in the solid and liquid material, the gas, and the graphite crucible, k_f and k_{gr} are the
 120 effective thermal conductivity of material inside the pilot furnace and the graphite crucible, with β a radiative
 121 constant associated with radiation between furnace particles, estimated assuming black body radiation and
 122 a typical distance between solid particles of 1 mm. dH_j is the rate of heat release for reaction j (and
 123 is negative for endothermic reactions). $F(z)$ is a function representing external heating into the graphite
 124 crucible from the induction heater. For simplicity, in the model analysis in [21] this function was taken to
 125 be $F(z) = Q\mathcal{H}(h_T - z)$, where Q is a scalar representing the heating strength per unit volume, \mathcal{H} is the
 126 Heaviside function, and the pilot furnace is being heated up to some fixed height h_T . In Section 4.1 we will
 127 use this function to ease the analysis of the resulting series solution. However, a different functional form
 128 of $F(z)$ could readily be used, and in particular in Section 4.2 and 4.3 our asymptotic solutions require an
 129 invertible $F(z)$. When a specific heating profile is needed in these sections we will use the smooth function
 130 $F(z) = \frac{Q}{2}(1 + \tanh(\mu(h_T - z)))$, which tends to a multiple of the Heaviside function as $\mu \rightarrow \infty$. The k_j
 131 in (9) are reaction constants, and the $P_j(T)$ are partial pressure functions of temperature, which limit the
 132 appropriate reactions. Note that r_C represents the reactivity of carbon, which could vary with different raw
 133 materials used and also during furnace operation. For simplicity, in this model r_C is taken to be a constant
 134 between zero and one. Similarly, for simplicity, the contact surface is not considered in reactions R_{-2} , R_4 ,
 135 or R_5 , which are between two liquids, a gas and a solid, and a liquid and a solid, respectively. Finally,
 136 $T_M = 1996 \text{ K}$ is the dimensional melting temperature of quartz [2]. Several of the reaction rates in (9) are
 137 not smooth. As can be seen in Figure 7 of paper [21], for such reactions the spatial domain is divided into
 138 regions where the reaction occurs and where it does not occur. This is exploited in Section 3 of this paper.

139 From now on we take $U_s = 0$, since we consider behaviour within the pilot furnace experiment where
 140 material is not fed in to the top of the furnace. Our model has the initial conditions

$$141 \quad (10) \quad \begin{aligned} C_C &= c_0, & C_{\text{SiC}} &= 0, & C_{\text{SiO}_2(s)} &= c_0\alpha, & C_{\text{SiO}_2(l)} &= 0, & C_{\text{Si}} &= 0, & P &= \frac{P_{\text{TOT}}}{2}, & U_g &= 0, & T &= 300, \\ C_g &= \frac{P_{\text{TOT}}}{300R} \left(1 - c_0 \left(\frac{M_C}{\rho_C} + \frac{M_{\text{SiO}_2(s)}}{\rho_{\text{SiO}_2(s)}} \alpha \right) \right), \end{aligned}$$

142 at $t = 0$, where $c_0 = 38000 \text{ mol/m}^3$ and $\alpha = 0.454$ are measured from the experiment. We also have the
 143 boundary conditions

$$144 \quad (11) \quad U_g(0, t) = 0, \quad \frac{\partial T(0, t)}{\partial z} = 0, \quad \frac{\partial T(1, t)}{\partial z} = 0.$$

145 Note there is no boundary condition for $U_g(1, t)$ because gas is free to leave the top of the furnace.

146 In [21] we performed numerical simulations of this model to replicate behaviour in the pilot furnace and
 147 conducted parameter sweeps to see the influence of various input parameters on output metrics of the silicon
 148 yield, the SiO losses and solid build-up. As in [21], all numerical simulations in this paper are found using
 149 first order finite difference schemes, with upwinding for convective fluxes and the timestep chosen to obey the
 150 Courant-Friedrichs-Lewy (CFL) condition. There is, however, much to be learned by exploiting the relative
 151 sizes of the various parameters that are found in the model to determine the asymptotic behaviour. Many
 152 of the parameters in the model are not known accurately, but have been calibrated with industrial furnaces
 153 to give sensible results from previous models (see the dynamic model [8] and SiMod [23]). Thus finding the
 154 general qualitative behaviour when certain parameters are small or large helps to understand the interplay
 155 of the chemical, thermal, and transport effects.

156 We choose to write the dimensionless model in terms of the timescale of the melting reaction R_3 ,
 157 $\tau = (k_3 T_0)^{-1}$, where $T_0 = 1000$ K is the typical temperature difference between the top and bottom of the
 158 furnace. In the numerical simulations shown in [21] we find that the concentrations of SiC, SiO₂(l), and Si
 159 remain around 30 times smaller than the concentrations of C and SiO₂(s). Also, the concentration of gas is
 160 around 10⁴ times smaller than the concentrations of C and SiO₂(s). We thus seek parameters ϵ and δ such
 161 that the concentrations of SiC, SiO₂(l), and Si are $\mathcal{O}(\epsilon)$, and the concentration of gas is $\mathcal{O}(\delta)$. A scale for
 162 ϵ emerges by considering a balance between reactions R_3 and R_5 . Liquid quartz is formed through R_3 and
 163 then reacts with C through R_5 to form CO and SiO. We let ϵ be the ratio of the rate of R_3 to R_5 , or ratio
 164 of the timescale of R_5 to R_3 . We let δ be the ratio of time taken for the gas to convect the height of the
 165 furnace to the timescale for R_3 . We thus have

$$166 \quad (12) \quad \epsilon = \frac{k_3 T_0}{k_5 c_0} = \frac{1/k_5 c_0}{1/k_3 T_0}, \quad \delta = \frac{h/V}{1/k_3 T_0},$$

167 where h is the height of the furnace and V is a typical value of the magnitude of the gas velocity. We
 168 have $0 < \delta \ll \epsilon \ll 1$ and will consider the joint limits $\epsilon \rightarrow 0$ and $\delta \rightarrow 0$, with $\delta/\epsilon \rightarrow 0$. The limit $\epsilon \rightarrow 0$
 169 corresponds to the reaction between carbon and SiO₂(l) being instantaneous when compared to the melting
 170 of SiO₂(l), so that as soon as quartz melts to liquid quartz it reacts with any available carbon. The limit
 171 $\delta \rightarrow 0$ corresponds to instantaneous gas flow when compared with the melting of quartz, but as $\delta/\epsilon \rightarrow 0$,
 172 this gas flow is also faster than the chemical timescale for R_5 .

173 We thus utilise the dimensionless scalings

$$174 \quad (13) \quad \begin{aligned} C_C &= c_0 \bar{C}_C, \quad C_{\text{SiO}_2(s)} = c_0 \bar{C}_{\text{SiO}_2(s)}, \quad C_{\text{SiC}} = \epsilon c_0 \bar{C}_{\text{SiC}}, \quad C_{\text{SiO}_2(l)} = \epsilon c_0 \bar{C}_{\text{SiO}_2(l)}, \quad C_{\text{Si}} = \epsilon c_0 \bar{C}_{\text{Si}}, \quad C_g = \delta c_0 \bar{C}_g, \\ T &= (T_{\text{bottom}} - T_{\text{top}}) \bar{T} + T_{\text{top}}, \quad t = \tau \bar{t}, \quad z = h \bar{z}, \quad U_g = V \bar{U}_g, \quad P = P_{\text{TOT}} \bar{P}, \quad P_j = P_{\text{TOT}} \bar{P}_j, \\ \sigma_s &= c_0 C_{p,C} \bar{\sigma}_s, \quad \sigma_g = \delta c_0 C_{p,C} \bar{\sigma}_g, \quad F(z) = Q \bar{F}(\bar{z}), \end{aligned}$$

175 where $T_{\text{bottom}} = 2400$ K and $T_{\text{top}} = 1400$ K are typical temperatures found at the bottom and the top of the
 176 furnace, and $C_{p,C}$ is the specific heat of carbon. Dropping the overbar notation we have the dimensionless
 177 equations

$$178 \quad (14) \quad \frac{\partial}{\partial t} \begin{pmatrix} C_C \\ \epsilon C_{\text{SiC}} \\ C_{\text{SiO}_2(s)} \\ \epsilon C_{\text{SiO}_2(l)} \\ \epsilon C_{\text{Si}} \\ \delta C_g(1-P) \\ \delta C_g P \end{pmatrix} + \frac{\partial}{\partial z} \begin{pmatrix} 0 \\ 0 \\ 0 \\ 0 \\ 0 \\ U_g C_g(1-P) \\ U_g C_g P \end{pmatrix} = \begin{pmatrix} -2 & 0 & 0 & 0 & 0 & -1 \\ 1 & 0 & 0 & 0 & -1 & 0 \\ 0 & 0 & 0 & -1 & 0 & 0 \\ 0 & 1 & -1 & 1 & 0 & -1 \\ 0 & 1 & -1 & 0 & 2 & 0 \\ 1 & 0 & 0 & 0 & 1 & 1 \\ -1 & -2 & 2 & 0 & -1 & 1 \end{pmatrix} \begin{pmatrix} \epsilon r_1 \\ \epsilon r_2 \\ \epsilon r_{-2} \\ r_3 \\ \epsilon r_4 \\ r_5 \end{pmatrix},$$

179

$$180 \quad (15) \quad g_0 \left(T + \frac{T_{\text{top}}}{T_0} \right) C_g + m_C C_C + \epsilon m_{\text{SiC}} C_{\text{SiC}} + m_{\text{SiO}_2(s)} C_{\text{SiO}_2(s)} + \epsilon m_{\text{SiO}_2(l)} C_{\text{SiO}_2(l)} + \epsilon m_{\text{Si}} C_{\text{Si}} = 1,$$

181

$$182 \quad (16) \quad \begin{aligned} &\frac{\partial}{\partial t} \left(\left(T + \frac{T_{\text{top}}}{T_0} \right) (\sigma_s + \delta \sigma_g + \sigma_{gr}^*) \right) + \frac{\partial}{\partial z} \left(\left(T + \frac{T_{\text{top}}}{T_0} \right) U_g \sigma_g \right) \\ &= a \frac{\partial^2 T}{\partial z^2} + \beta^* \frac{\partial}{\partial z} \left(\left(\frac{T_{\text{top}}}{T_0} + T \right)^3 \frac{\partial T}{\partial z} \right) + \epsilon (\gamma_1 r_1 + \gamma_2 r_2 + \gamma_{-2} r_{-2} + \gamma_4 r_4) + \gamma_5 r_5 + qF, \end{aligned}$$

183 where

$$184 \quad (17) \quad \begin{pmatrix} r_1 \\ r_2 \\ r_{-2} \\ r_3 \\ r_4 \\ r_5 \end{pmatrix} = \begin{pmatrix} \chi_1 C_C (P - P_1(T))^+ \\ \chi_2 (P - P_2(T))^+ \\ \chi_{-2} C_{\text{SiO}_2(l)} C_{\text{Si}} \\ C_{\text{SiO}_2(s)} (T - T_m)^+ \\ \chi_4 C_{\text{SiC}} (P - P_4(T))^+ \\ C_{\text{SiO}_2(l)} C_C \end{pmatrix},$$

185 (18) $\sigma_s = C_C + \epsilon C_{\text{SiC}} C_{P,\text{SiC}/C} + C_{\text{SiO}_2(\text{s})} C_{P,\text{SiO}_2(\text{s})/C} + \epsilon C_{\text{SiO}_2(\text{l})} C_{P,\text{SiO}_2(\text{l})/C} + \epsilon C_{\text{Si}} C_{P,\text{Si}/C},$

186

187 (19) $\sigma_g = C_g \left((1 - P) C_{P,\text{CO}/C} + P C_{P,\text{SiO}/C} \right), \quad g_0 = \delta \frac{RT_0 c_0}{P_{\text{TOT}}}, \quad m_X = c_0 \frac{M_X}{\rho_X}.$

188 We have scaled the kinetic rates χ_j such that each is an order one constant, taking a typical value $r_C = 0.2$
 189 [21] when choosing the appropriate scale for r_1 . Each variable and parameter listed in the equations above
 190 is order one. g_0 is an order one constant, since $RT_0 c_0 / P_{\text{TOT}}$ is $\mathcal{O}(\delta^{-1})$ with $T_0 := T_{\text{bottom}} - T_{\text{top}}$, as are the
 191 m_X . We have used the shorthand notation $C_{P,X/C} := C_{P,X} / C_{P,C}$ in the heat capacities σ_s and σ_g . T_m is
 192 the dimensionless melting temperature of quartz. There is no heat release associated with r_3 in the model,
 193 so there is no γ_3 .

194 We have the dimensionless initial conditions (for $0 \leq z \leq 1$)

195 (20)
$$C_C = 1, \quad C_{\text{SiC}} = 0, \quad C_{\text{SiO}_2(\text{s})} = \alpha, \quad C_{\text{SiO}_2(\text{l})} = 0, \quad C_{\text{Si}} = 0, \quad P = \frac{1}{2}, \quad U_g = 0, \quad T = -1.1,$$

$$C_g = \frac{P_{\text{TOT}}}{300R} \left(\frac{1}{c_0} - \left(\frac{M_C}{\rho_C} + \frac{M_{\text{SiO}_2(\text{s})}}{\rho_{\text{SiO}_2(\text{s})}} \alpha \right) \right),$$

196 at $t = 0$, with the dimensionless boundary conditions remaining the same as the dimensional boundary
 197 conditions given in (11).

198 To understand the behaviour of solutions to our model (14) - (20) we begin by constraining the tempera-
 199 ture to be fixed, with a prescribed steady state temperature $T(z)$ considered in Section 3, and we neglect the
 200 energy equation (16). Although neither pilot or industrial furnaces operate with a steady state temperature,
 201 this allows us to focus on the chemical and gas transport dynamics, and makes the analysis more tractable.
 202 In Section 4 we will return to the problem with time-variable temperature. Although less analytical progress
 203 can then be made, the simplifications developed allow for a reduced model to be identified.

204 **3. Prescribed Temperature Asymptotics.** We analyse the dimensionless equations (14) - (15), but
 205 with a prescribed temperature profile $T(z)$ instead of the energy equation (16). Initial conditions (20) and
 206 boundary conditions (11) are used for concentrations, partial pressure, and gas velocity. Where possible we
 207 will work in terms of a general $T(z)$, but any time a specific profile is used we will utilise the piecewise linear
 208 profile $T(z) = \min\left(1, \frac{1-z}{1-h_T^*}\right)$. With this function the furnace is at constant unitary temperature up to a
 209 dimensionless height $h_T^* = 0.544$, and above this height linearly decays to zero at the top of the furnace.
 210 This is to replicate the experimental behaviour, where the induction furnace creates a temperature gradient
 211 by inputting more heat into the bottom of the furnace (see [21]).

212 There are different spatial regions in the problem, due to the behaviour of the melting reaction $r_3 =$
 213 $C_{\text{SiO}_2(\text{s})}(T - T_m)^+$. In the lower, hotter part of the furnace $T > T_m$ and hence $r_3 = \mathcal{O}(1)$. In the upper, colder
 214 region of the furnace $T < T_m$ and hence $r_3 = 0$. These regions are separated by the interface given by the
 215 isotherm $T = T_m$. With a prescribed temperature profile we do not consider any temperature transient as it
 216 heats from cold, but process start from the prescribed hot profile. Hence the chemistry has a rapid transient
 217 period before getting near typical operating conditions. There are thus four main regimes of behaviour of
 218 the chemistry in height-time space, which are shown in Figure 2.

219 There is a separation between the blue region, where the temperature is too cold for solid quartz to melt,
 220 and the red region where quartz melts. There is also a separation between the early time regions (shown as
 221 hashed), where the pilot furnace moves away from the initial conditions to dynamics more likely to be seen
 222 in the industrial furnace, and the $\mathcal{O}(1)$ time regions (shown as solid). Since in all practical situations $U_g \geq 0$,
 223 and we have assumed no solid or liquid motion, we have that information propagates upwards in Figure 2 (so
 224 from Region II to Region I) as well as rightwards (from Region a to Region b). We now give details of the
 225 behaviour in each region found through expanding each variable in terms of the small parameter ϵ . That is
 226 for a variable Y we have $Y = Y^0 + \epsilon Y^1 + \mathcal{O}(\epsilon^2)$. We begin by considering Region II, since the gas produced
 227 in this region influences the dynamics in Region I. We find analytic solutions in Regions IIa and IIb and,
 228 where appropriate, give composite solutions that replicate both the inner and outer time behaviour. We then
 229 examine the upper part of the furnace, which is Region I. In Region Ia we list the leading order equations,

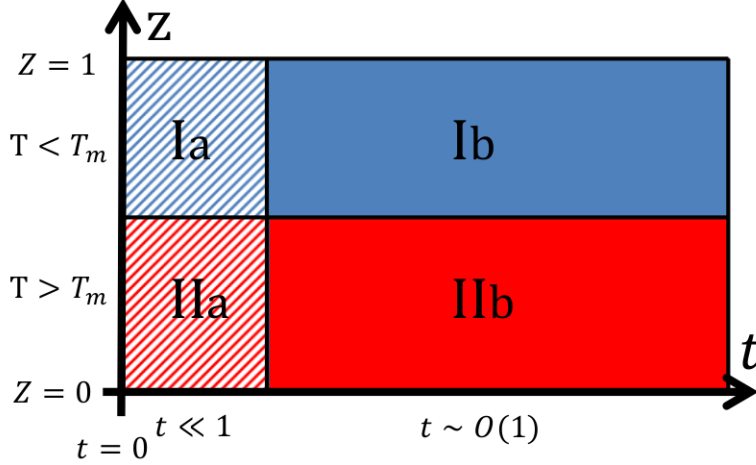


Fig. 2: Schematic of asymptotic regimes. Hashed regions correspond to early time and solid regions to larger time. The blue region, where the temperature is below the melting point of quartz, corresponds to the furnace charge. The red region, where melting of quartz occurs, corresponds to the mixed cavity and crater region in the model.

230 but find that the solid and liquid concentrations are solved by the initial conditions. Hence the corresponding
 231 leading order equations arising in Region Ib can be solved with these initial conditions, and analytic solutions
 232 are found for all of Region I. Matching occurs between Regions I and II in terms of continuity of the gas flux
 233 across the interface $T = T_m$. We give a summary of the main asymptotic behaviour in each region, but do
 234 not include all the details. A summary of leading and first order solutions is given in the appendix.

235 **3.1. Region IIa - early time cavity and crater.** We find that the appropriate timescale is $t = \hat{t}$,
 236 where \hat{t} is an order one variable. With this rescaling we find that the leading order equations from the matrix
 237 system (14) are at $\mathcal{O}(\epsilon^{-1})$ and are given by

$$238 \quad (21) \quad \frac{1}{\epsilon} \frac{\partial C_C^0}{\partial \hat{t}} = \mathcal{O}(1), \quad \frac{1}{\epsilon} \frac{\partial C_{\text{SiO}_2(\text{s})}^0}{\partial \hat{t}} = \mathcal{O}(1),$$

239 which have solutions $C_C^0 = 1$ and $C_{\text{SiO}_2(\text{s})}^0 = \alpha$. We use these when finding the leading order terms for the
 240 other variables. For the concentrations of SiC, SiO₂(l), and Si we have

$$241 \quad (22) \quad \frac{\partial C_{\text{SiC}}^0}{\partial \hat{t}} = \mathcal{O}(\epsilon), \quad \frac{\partial C_{\text{SiO}_2(\text{l})}^0}{\partial \hat{t}} = \alpha(T - T_m) - C_{\text{SiO}_2(\text{l})}^0 + \mathcal{O}(\epsilon), \quad \frac{\partial C_{\text{Si}}^0}{\partial \hat{t}} = \mathcal{O}(\epsilon).$$

242 With the zero initial conditions we have $C_{\text{SiC}}^0 = 0$, $C_{\text{Si}}^0 = 0$, and

$$243 \quad (23) \quad C_{\text{SiO}_2(\text{l})}^0 = \alpha(T(z) - T_m) \left(1 - e^{-\hat{t}}\right) = \alpha(T(z) - T_m) \left(1 - e^{-t/\epsilon}\right).$$

244 We can find the leading order gas flux $U_g^0 C_g^0$ and pressure P^0 from the equations

$$245 \quad (24) \quad \frac{\partial}{\partial z} (U_g^0 C_g^0 (1 - P^0)) = C_{\text{SiO}_2(\text{l})}^0 + \mathcal{O}(\epsilon), \quad \frac{\partial}{\partial z} (U_g^0 C_g^0 P^0) = C_{\text{SiO}_2(\text{l})}^0 + \mathcal{O}(\epsilon).$$

246 Utilising the no-flux boundary condition $U_g(0, \hat{t}) = 0$, we can add the above equations and integrate to find

$$247 \quad (25) \quad U_g^0 C_g^0 = 2\alpha \left(1 - e^{-t/\epsilon}\right) \int_{y=0}^{y=z} (T(y) - T_m) dy,$$

248 and hence $P^0 = \frac{1}{2}$. We can find C_g^0 from the reduced, leading order no-voids condition

$$249 \quad (26) \quad g_0 \left(T + \frac{T_{\text{top}}}{T_0}\right) C_g^0 + m_C + m_{\text{SiO}_2(\text{s})} \alpha + \mathcal{O}(\epsilon) = 1,$$

250 so that for prescribed $T(z)$

$$251 \quad (27) \quad C_g^0 = \frac{1 - m_C - m_{\text{SiO}_2(\text{s})}\alpha}{g_0 \left(T(z) + \frac{T_{\text{top}}}{T_0} \right)}.$$

252 Thus the concentration of gas increases as the temperature decreases higher up in the furnace. The leading
 253 order gas velocity U_g^0 can then be found using (25) and (27). Note that on an even smaller $\mathcal{O}(\delta)$ timescale
 254 different behaviour would be found, with the time derivative of $C_g^0(1 - P^0)$ and $C_g^0 P^0$ balancing with the
 255 convective flux and reaction r_5^0 . However, the resulting wave-like behaviour only describes the very fast
 256 transient behaviour of the gas flux and pressure and so is not discussed for the sake of brevity.

257 **3.2. Region IIb - order one time crater and cavity.** We next examine behaviour in the outer-in-
 258 time crater and cavity region. Here we have the order one timescale t . The order one equations are found
 259 to be

$$260 \quad (28) \quad \frac{\partial C_C^0}{\partial t} = -r_5^0, \quad \frac{\partial C_{\text{SiO}_2(\text{s})}^0}{\partial t} = -r_3^0, \quad 0 = r_3^0 - r_5^0, \quad \frac{\partial}{\partial z} (U_g^0 C_g^0 (1 - P^0)) = r_5^0, \quad \frac{\partial}{\partial z} (U_g^0 C_g^0 P^0) = r_5^0,$$

261 which all have $\mathcal{O}(\epsilon)$ corrections, and the no-voids equation is

$$262 \quad (29) \quad g_0 \left(T + \frac{T_{\text{top}}}{T_0} \right) C_g^0 + m_C C_C^0 + m_{\text{SiO}_2(\text{s})} C_{\text{SiO}_2(\text{s})}^0 = 1 + \mathcal{O}(\epsilon).$$

263 From the third equation in (28) we have a leading order balance between the melting of quartz r_3^0 and the
 264 production of CO and SiO gas from liquid quartz and carbon, r_5^0 . This corresponds to a quasi-steady state
 265 assumption, since the time rate of change of liquid quartz is an order smaller than the reaction rates r_3 and
 266 r_5 . This reaction balance was the motivation for choosing $\epsilon = k_3 T_0 / k_5 c_0$ and scaling the concentrations of
 267 SiC, SiO₂(s), and Si to be $\mathcal{O}(\epsilon)$ in Section 2. We have the reaction rate $r := r_3^0 = r_5^0$ from this balance, and
 268 find it is easiest to work with

$$269 \quad (30) \quad r := C_{\text{SiO}_2(\text{s})}^0 (T - T_m).$$

270 As the leading order terms for the concentrations of carbon and solid quartz in Region IIa are the initial
 271 conditions, the solutions in Region IIb can be found to be

$$272 \quad (31) \quad C_C^0 = \alpha e^{-(T-T_m)t} + (1 - \alpha), \quad C_{\text{SiO}_2(\text{s})}^0 = \alpha e^{-(T-T_m)t}.$$

273 In Figure 3 we compare these solutions with the numerical results for a simulation with a fixed temperature
 274 profile, showing a good fit. We can find $C_{\text{SiO}_2(\text{l})}^0$ from the balance between r_3^0 and r_5^0 to give

$$275 \quad (32) \quad C_{\text{SiO}_2(\text{l})}^0 = \frac{C_{\text{SiO}_2(\text{s})}^0 (T - T_m)}{C_C^0} = \frac{(T - T_m) \alpha e^{-(T-T_m)t}}{\alpha e^{-(T-T_m)t} + (1 - \alpha)}.$$

276 Although this tends to zero as t increases, it does not satisfy the initial condition of $C_{\text{SiO}_2(\text{l})} = 0$. This is
 277 accounted for in Section 3.1 where the early time behaviour was examined.

278 To find the gas flux we add the last two equations in (28) and integrate spatially, applying the no-flux
 279 boundary condition $U_g^0(0, t) = 0$, to give

$$280 \quad (33) \quad U_g^0(z, t) C_g^0(z, t) = 2\alpha \int_{y=0}^{y=z} e^{-(T(y)-T_m)t} (T(y) - T_m) dy = -2\alpha \frac{\partial}{\partial t} \int_{y=0}^{y=z} e^{-(T(y)-T_m)t} dy.$$

281 We can find the leading order pressure by integrating the last equation in (28) and noting

$$282 \quad (34) \quad U_g^0 C_g^0 P^0 = \frac{1}{2} U_g^0 C_g^0 + g(t).$$

283 The arbitrary function of time $g(t)$ is zero from the no-flux boundary condition for velocity, and since
 284 $U_g^0 C_g^0 \neq 0$ in general, we again have $P^0 = \frac{1}{2}$.

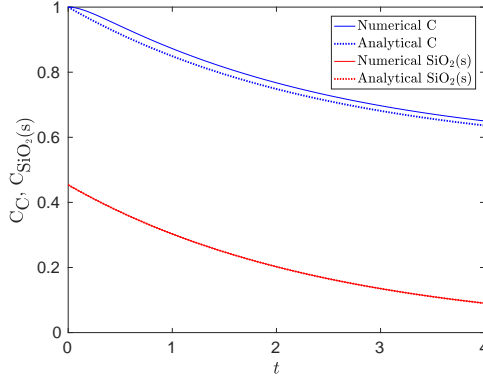


Fig. 3: Dimensionless concentration of carbon, in blue, and solid quartz, in red, at height $z = 0.3$. We compare numerical solutions of the full system with $T(z)$ in solid lines to asymptotic solution in dashed lines, with parameter values $\epsilon = 0.16$, $\delta = 3.2 \times 10^{-4}$, and $\alpha = 0.45$.

285 We can find the concentration of gas through equation (29), giving

$$286 \quad (35) \quad C_g^0 = \frac{1}{g_0 \left(T + \frac{T_{\text{top}}}{T_0} \right)} \left(1 - (m_C + m_{\text{SiO}_2(\text{s})}) \alpha e^{-(T-T_m)t} - m_C(1-\alpha) \right).$$

287 Notice that although this is not a separable solution, we can decompose it as $C_g^0(z, t) = X(z)Y(t, z)$ for

$$288 \quad (36) \quad X(z) := \frac{1}{g_0 \left(T + \frac{T_{\text{top}}}{T_0} \right)}, \quad Y(t, z) := 1 - (m_C + m_{\text{SiO}_2(\text{s})}) \alpha e^{-(T-T_m)t} - m_C(1-\alpha).$$

289 Thus $Y(0, z) = 1 - m_{\text{SiO}_2(\text{s})}\alpha - m_C$ and $Y(t, z) \rightarrow 1 - m_C(1-\alpha)$ as $t \rightarrow \infty$. This means that there is a
 290 saturation level for the gas concentration, which happens as the concentrations of carbon and solid quartz
 291 tend towards their long time behaviour.

292 If required, we could calculate the velocity from the solutions for the gas flux and the gas concentration.
 293 For example, using our specific example temperature profile $T(z) = \min \left(1, \frac{1-z}{1-h_T^*} \right)$, in the region $0 \leq z \leq h_T^*$
 294 where $T(z) \equiv 1$, we have

$$295 \quad (37) \quad U_g^0(z, t) = 2\alpha \frac{(1-T_m)e^{-(1-T_m)t}z}{C_g^0(z, t)}.$$

296 We can find composite asymptotic solutions valid for all time by combining our inner-in-time and outer-
 297 in-time solutions. Letting y_I denote an inner solution, y_O an outer solution, and y_{overlap} the overlap, we
 298 have that the composite solution y_c is given by $y_c = y_I + y_O - y_{\text{overlap}}$. The composite solution for the
 299 concentration of $\text{SiO}_2(\text{l})$ is thus

$$300 \quad (38) \quad C_{\text{SiO}_2(\text{l})}^0 = \alpha(T-T_m) \left[\frac{e^{-(T-T_m)t}}{\alpha e^{-(T-T_m)t} + (1-\alpha)} - e^{-\frac{t}{\epsilon}} \right].$$

301 Similarly for the gas flux we have

$$302 \quad (39) \quad U_g^0(z, t)C_g^0(z, t) = 2\alpha \int_{y=0}^{y=z} (T(y) - T_m) \left(e^{-(T(y)-T_m)t} - e^{-\frac{t}{\epsilon}} \right) dy.$$

303 In Figure 4 we compare the early time, late time, and composite asymptotics with numerics for the full
 304 system, for the concentration of liquid quartz and the gas flux. The numerical and composite asymptotic

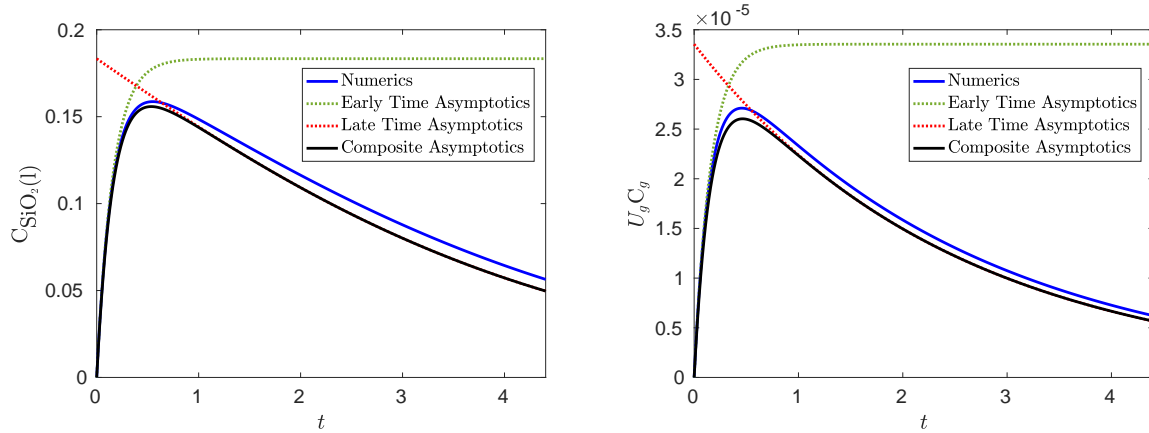


Fig. 4: Comparison of early time, late time, and composite asymptotics, with numerics of the full system with prescribed temperature profile at height $z = 0.3$. On the left is the concentration of liquid quartz and on the right is the gas flux (both dimensionless). Parameter values used are $\epsilon = 0.16$, $\delta = 3.2 \times 10^{-4}$, $\alpha = 0.45$, $\chi_1 = 0.15$, and $\chi_2 = 0.25$.

305 curves match in long time, as the variables go to zero. The difference between the curves is due to reactions
 306 r_2 and r_{-2} , which do not appear in the leading order asymptotics.

307 The equations for the leading order concentrations of SiC and Si are

$$308 \quad (40) \quad \epsilon \frac{\partial C_{\text{SiC}}^0}{\partial t} = \epsilon \chi_1 \left(\alpha e^{-(T-T_m)t} + (1-\alpha) \right) \left(\frac{1}{2} - P_1 \right)^+ - \epsilon \chi_4 C_{\text{SiC}}^0 \left(\frac{1}{2} - P_4 \right)^+ + \mathcal{O}(\epsilon^2),$$

309

$$310 \quad (41) \quad \epsilon \frac{\partial C_{\text{Si}}^0}{\partial t} = \epsilon \chi_2 \left(\frac{1}{2} - P_2 \right)^+ - \epsilon \chi_{-2} \left(\frac{(T-T_m)\alpha e^{-(T-T_m)t}}{\alpha e^{-(T-T_m)t} + (1-\alpha)} \right) C_{\text{Si}}^0 + 2\epsilon \chi_4 C_{\text{SiC}}^0 \left(\frac{1}{2} - P_4 \right)^+ + \mathcal{O}(\epsilon^2).$$

311 These, along with the the zero initial conditions (20), could be solved analytically by first solving (40) and
 312 then substituting this into (41). In the typical temperature range found in Region II we find $P_1 < \frac{1}{2}$, but P_2
 313 and P_4 can be smaller or larger than $\frac{1}{2}$, and so the different cases would need to be considered individually.
 314 We do not include these cases here.

315 **3.3. Region Ia - early time furnace charge.** We now consider the upper region in the furnace,
 316 which corresponds to the furnace charge. In this region $T < T_m$ so the solid quartz does not melt, and
 317 $r_3 \equiv 0$. Hence $C_{\text{SiO}_2(s)} = \alpha$ for all time and we now have seven equations for the remaining seven unknowns,
 318 being the concentrations of C, SiC, $\text{SiO}_2(l)$, Si, and gas, the partial pressure P , and the gas flux U_g . We
 319 begin with Region Ia, where we analyse the early time behaviour. Using the same timescale as in Region
 320 IIa, $t = \hat{t}$, we find the leading order equations for each variable are given by

$$321 \quad (42) \quad \frac{1}{\epsilon} \frac{\partial C_{\text{C}}^0}{\partial \hat{t}} = \mathcal{O}(1), \quad \frac{\partial C_{\text{SiC}}^0}{\partial \hat{t}} = \mathcal{O}(\epsilon), \quad \frac{\partial C_{\text{SiO}_2(l)}^0}{\partial \hat{t}} = -r_5^0 + \mathcal{O}(\epsilon), \quad \frac{\partial C_{\text{Si}}^0}{\partial \hat{t}} = \mathcal{O}(\epsilon),$$

322

$$323 \quad (43) \quad \frac{\partial}{\partial z} (U_g^0 C_g^0 (1 - P^0)) = r_5^0 + \mathcal{O}(\epsilon), \quad \frac{\partial}{\partial z} (U_g^0 C_g^0 P^0) = r_5^0 + \mathcal{O}(\epsilon),$$

324

$$325 \quad (44) \quad g_0 \left(T + \frac{T_{\text{top}}}{T_0} \right) C_g^0 + m_{\text{C}} C_{\text{C}}^0 + m_{\text{SiO}_2(s)} \alpha = 1 + \mathcal{O}(\epsilon).$$

326 Clearly $C_{\text{C}}^0 = 1$, $C_{\text{SiC}}^0 = 0$, and $C_{\text{Si}}^0 = 0$. Since $r_5^0 = C_{\text{C}}^0 C_{\text{SiO}_2(l)}^0 = C_{\text{SiO}_2(l)}^0$ we find the third equation in (42)
 327 leads to $C_{\text{SiO}_2(l)}^0 = 0$, since the pre-exponential factor is zero from the initial condition. Thus the leading

328 order concentrations of the solid and liquid species are given by their initial conditions, and they do not alter
 329 significantly in the early time. When analysing their dynamics in Region Ib we will use initial conditions for
 330 the whole model (20). Similarly, since $C_C^0 = 1$ and $C_{\text{SiO}_2(\text{s})}^0 = \alpha$, C_g^0 is constant, given by (44). We then find
 331 that $U_g^0 C_g^0$ and P^0 are both functions of time only, since $r_5^0 = 0$. We can find these functions by imposing
 332 continuity of the gas flux and pressure across the interface $z = z_m$ (which is $z : T(z) = T_m$) and utilising
 333 solutions from Region IIa below. Hence $P^0 = \frac{1}{2}$ and

$$334 \quad (45) \quad U_g^0 C_g^0 = 2\alpha \left(1 - e^{-t/\epsilon}\right) \int_{y=0}^{y=z_m} (T(y) - T_m) dy,$$

335 where we have used the gas flux at $z = z_m$ from (25).

336 **3.4. Region Ib - order one time furnace charge.** We now consider order one time behaviour in the
 337 upper furnace, where $T < T_m$. We find the leading order equations for the solid and liquid concentrations
 338 are

$$339 \quad (46) \quad \frac{\partial C_C^0}{\partial t} = -r_5^0 + \mathcal{O}(\epsilon), \quad \epsilon \frac{\partial C_{\text{SiC}}^0}{\partial t} = \epsilon r_1^0 - \epsilon r_4^0 + \mathcal{O}(\epsilon^2), \quad 0 = -r_5^0 + \mathcal{O}(\epsilon), \quad \epsilon \frac{\partial C_{\text{Si}}^0}{\partial t} = \epsilon r_2^0 - \epsilon r_{-2}^0 + \epsilon r_4^0 + \mathcal{O}(\epsilon^2),$$

340 along with the gas flux equations (43) and the reduced no-voids equation (44) from Region Ia. Since $r_5^0 = 0$,
 341 then $C_C^0 = 1$ and the partial pressure and gas flux are again given by imposing continuity from below, this
 342 time with Region IIb, to give $P^0 = \frac{1}{2}$, and

$$343 \quad (47) \quad U_g^0 C_g^0 = 2\alpha \int_{y=0}^{y=z_m} e^{-(T(y)-T_m)t} (T(y) - T_m) dy,$$

344 using (33). Also, since $r_5^0 = 0$ and $r_5^0 = C_C^0 C_{\text{SiO}_2(\text{l})}^0$, then $C_{\text{SiO}_2(\text{l})}^0 = 0$, and hence $r_{-2}^0 = \chi_{-2} C_{\text{SiO}_2(\text{l})}^0 C_{\text{Si}}^0 = 0$.
 345 We now examine the $\mathcal{O}(\epsilon)$ equations for the concentrations of solid and liquid species,

$$346 \quad (48) \quad \frac{\partial C_C^1}{\partial t} = -2r_1^0 - r_5^1 + \mathcal{O}(\epsilon), \quad \frac{\partial C_{\text{SiC}}^0}{\partial t} = r_1^0 - r_4^0 + \mathcal{O}(\epsilon), \quad 0 = r_2^0 - r_5^1 + \mathcal{O}(\epsilon), \quad \frac{\partial C_{\text{Si}}^0}{\partial t} = r_2^0 + 2r_4^0 + \mathcal{O}(\epsilon).$$

347 There is a balance between r_2 and r_5 , so that the liquid quartz, which condenses through r_2 , reacts with
 348 the available carbon through r_5 . Since reaction r_5 is limited by the amount of liquid quartz available, it is
 349 $\mathcal{O}(\epsilon)$ in the upper furnace, which is much smaller than the $\mathcal{O}(1)$ reaction in the lower furnace, in which the
 350 available liquid quartz is provided through reaction r_3 , the melting of solid quartz. Indeed, to order one no
 351 reactions take place in the furnace charge and the chemical species remain in their initial state. To find the
 352 $\mathcal{O}(\epsilon)$ changes to the chemical species we utilise the balance $r_2^0 = r_5^1$ and solutions $C_C^0 = 1$ and $P^0 = \frac{1}{2}$. In
 353 addition, when $T < T_m$ we have that $P_4 > \frac{1}{2}$, but $P_1, P_2 < \frac{1}{2}$ (see equilibrium partial pressure diagram in
 354 [18]). Hence, we have that

$$355 \quad (49) \quad \frac{\partial C_C^1}{\partial t} = -2\chi_1 \left(\frac{1}{2} - P_1\right) - \chi_2 \left(\frac{1}{2} - P_2\right), \quad \frac{\partial C_{\text{SiC}}^0}{\partial t} = \chi_1 \left(\frac{1}{2} - P_1\right), \quad \frac{\partial C_{\text{Si}}^0}{\partial t} = \chi_2 \left(\frac{1}{2} - P_2\right).$$

356 In Section 3.3 we only calculated C_C to first order, but we can easily find that in Region Ia $C_C^1 = 0$. Hence
 357 we can use the zero Dirichlet condition for C_C^1 in Region Ib, as well as for C_{SiC}^0 and C_{Si}^0 , to find

$$358 \quad (50) \quad C_C^1 = - \left(2\chi_1 \left(\frac{1}{2} - P_1\right) + \chi_2 \left(\frac{1}{2} - P_2\right)\right) t, \quad C_{\text{SiC}}^0 = \chi_1 \left(\frac{1}{2} - P_1\right) t, \quad C_{\text{Si}}^0 = \chi_2 \left(\frac{1}{2} - P_2\right) t.$$

359 We show comparisons of these solutions with numerics in Figure 5. We have that carbon is being lost to
 360 gas through reaction r_5 (reacting with the liquid quartz produced through r_2) and to silicon carbide through
 361 reaction r_1 . The production of silicon through r_2 is equal to the loss of carbon through r_5 , since all the
 362 available liquid quartz reacts with carbon (to leading order). The dynamics in the furnace charge are driven
 363 by the behaviour of convecting SiO molecules, which can condense through r_2 , leading to silicon production,
 364 react with carbon, through r_1 to produce silicon carbide, or convect out of the furnace unreacted. The

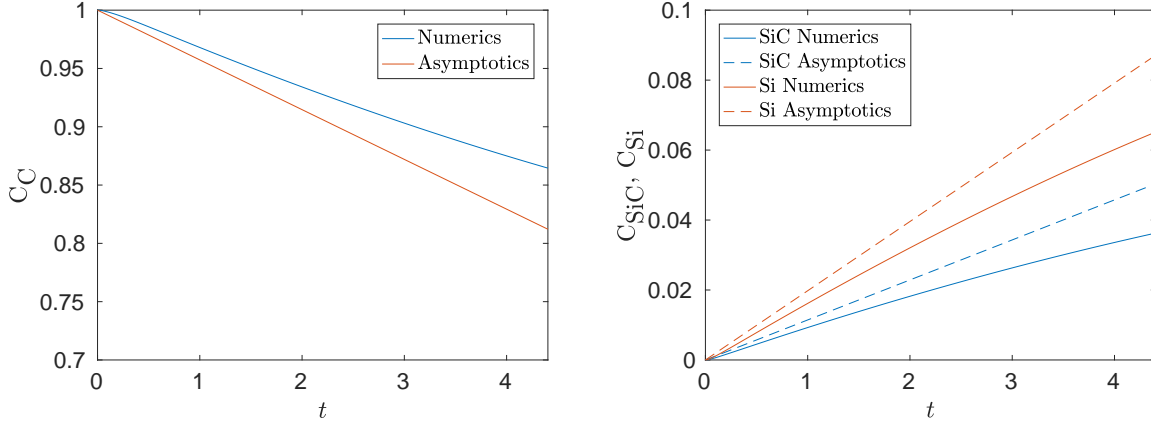


Fig. 5: Comparison of numerics and asymptotics at $z = 0.9$. On the left are plots of the dimensionless concentration of carbon, showing numerics in blue and asymptotics in red. On the right are plots of the dimensionless concentrations of SiC (in blue) and Si (in red), showing numerics in solid and asymptotics in dashed. There is agreement to $\mathcal{O}(\epsilon)$ but noticeable $\mathcal{O}(\epsilon^2)$ disagreement, which would be reduced by considering more terms. Notice that the scale for the left plot is between 0.7 and 1, so there is an approximate 5% error for C_C , and the scale on the right plot is only up to 0.1, so the absolute error for C_{SiC} and C_{Si} is also small, since these are order one dimensionless variables. Parameter values used are $\epsilon = 0.16$, $\delta = 3.2 \times 10^{-4}$, $\chi_1 = 0.15$, and $\chi_2 = 0.25$.

365 parameter $\lambda = \chi_2/\chi_1$ determines the relative importance of reactions r_1 and r_2 . The higher λ is, the more
 366 silicon will be produced. The lower λ is, the more silicon carbide will build up.

367 We now find the $\mathcal{O}(\epsilon)$ corrections to the gas flux and the pressure. Adding the last two rows in (14)
 368 gives an equation for the gas flux, which we treat as one variable (so that $U_g C_g = U_g^0 C_g^0 + \epsilon U_g^1 C_g^1 + \mathcal{O}(\epsilon^2)$).
 369 We have that $U_g^0 C_g^0 = f(t)$, given by (47), and find that

$$370 \quad (51) \quad \epsilon \frac{\partial}{\partial z} (U_g^1 C_g^1) = -2\epsilon r_2^0 + 2\epsilon r_5^1 + \mathcal{O}(\epsilon^2).$$

371 By the balance $r_2^0 = r_5^1$ in (48) we have that $U_g^1 C_g^1$ is also a function of time only, which could be given from
 372 matching with the region below, Region IIb, if we desired. The $\mathcal{O}(\epsilon)$ equation for P^1 is

$$373 \quad (52) \quad \epsilon \frac{\partial}{\partial z} (U_g^0 C_g^0 P^1 + U_g^1 C_g^1 P^0) = -\epsilon r_1^0 - 2\epsilon r_2^0 + \epsilon r_5^1 + \mathcal{O}(\epsilon^2),$$

374 where we have noted that $r_{-2}^0 = r_4^0 = 0$. Using $r_5^1 = r_2^0$, and since $U_g^0 C_g^0 = f(t)$ and $U_g^1 C_g^1 P^0$ are both
 375 spatially independent, we have

$$376 \quad (53) \quad f(t) \frac{\partial P^1}{\partial z} = - \left(\chi_1 \left(\frac{1}{2} - P_1(T(z)) \right) + \chi_2 \left(\frac{1}{2} - P_2(T(z)) \right) \right).$$

377 This implies

$$378 \quad (54) \quad P^1 = \frac{A(z)}{f(t)} + b(t),$$

379 where $A(z)$ is a decreasing function in z and $b(t)$ is an arbitrary function of time. Since $f(t) \rightarrow 0$ as $t \rightarrow \infty$
 380 this form of P^1 breaks down after long time. The timescale on which $P^1 = \mathcal{O}(\epsilon^{-1})$, thus breaking down the
 381 asymptotic expansion, is the timescale on which $f(t) = U_g^0 C_g^0$ given by (47) is $\mathcal{O}(\epsilon)$ (assuming $A(z) = \mathcal{O}(1)$).
 382 Assuming $M/2\alpha := \max|T'(y)|$ is an order one constant and letting $x := T(y) - T_m$, we have

$$383 \quad (55) \quad |f(t)| \leq M \left| \int_{x=0}^{1-T_m} x e^{-xt} dx \right| \leq M t^{-2},$$

384 and so this happens for $t = \mathcal{O}(\epsilon^{-1/2})$. In numerical simulations we find that $P \rightarrow P_2$ in long time behaviour,
 385 so that the condensation of SiO stops, but the reaction r_1 with carbon continues (as $P_2 > P_1$ [18]).

386 By prescribing a temperature profile $T(z)$ we have identified two spatial regions - a lower crater and
 387 cavity region, in which there is a balance between reactions r_3 and r_5 , and an upper furnace charge region in
 388 which chemical changes occur in smaller $\mathcal{O}(\epsilon)$ quantities and there is a balance between reactions r_2 and r_5 .
 389 By expanding variables in terms of the small parameter ϵ we have found analytic solutions throughout the
 390 furnace, with composite solutions for early time and order one time behaviour in Region II where appropriate.
 391 Information propagates upwards from the crater and cavity to the charge through the gas flux - an effect
 392 that we have quantified. In the charge there is competition between reactions r_1 , producing SiC, and r_2 ,
 393 producing Si.

394 **4. Full Model Asymptotics.** We now consider asymptotics of the full model, comprising of the
 395 equations (14) - (16), initial conditions (20), and boundary conditions (11). We utilise the balances developed
 396 in Section 3 and extend our analysis to consider a spatially and temporally varying temperature $T(z, t)$. In
 397 the pilot furnace experiments we see that the interface between the furnace charge and the cavity region
 398 rises as the furnace heats up. We would thus expect to have similar regions to Regions I and II as in Figure
 399 2, except that the interface $z = z_m$ moves with time. Considering the full model with varying temperature is
 400 thus important, because it captures this rising interface. In this section we reduce our model to two coupled
 401 equations for temperature and the concentration of solid quartz, which are dependent on three parameters.
 402 This simplified coupled model captures much of the qualitative behaviour of the full model, which has nine
 403 variables and over thirty parameters. We analyse early time behaviour, before reactions occur significantly,
 404 and consider the limit of small diffusion. We also comment on the joint limits of small diffusion and small
 405 external heating.

406 We consider leading order terms in the conservation of energy equation (16) in the limit $\epsilon \rightarrow 0$ and
 407 $\delta/\epsilon \rightarrow 0$. The superscript notation ⁰ used in Section 3 is dropped, with the assumption that all variables
 408 used to determine the simplified system are $\mathcal{O}(1)$. Although there are different equations in Regions I and
 409 II in Section 3, the changes in Region II are of higher order than in the other regions, so our leading order
 410 equations capture these effects primarily. To $\mathcal{O}(1)$ no chemical changes occur in the top of the furnace,
 411 but reactions and chemical transformations happen in the base. There is a balance between reactions r_3
 412 and r_5 in the furnace base, so we integrate the first two equations in (28) to get the algebraic relation
 413 $C_C = C_{\text{SiO}_2(\text{s})} + (1 - \alpha)$. Note that this does not hold in the top of the furnace, where carbon slowly decays
 414 but the concentration of solid quartz remains constant. However, this is an $\mathcal{O}(\epsilon)$ effect only. Noting that to
 415 leading order $P = \frac{1}{2}$, we then have

$$416 \quad (56) \quad \sigma_s = C_{\text{SiO}_2(\text{s})} (1 + C_{P,\text{SiO}_2(\text{s})/C}) + (1 - \alpha) + \mathcal{O}(\epsilon), \quad \sigma_g = \frac{1}{2} C_g (C_{P,\text{CO}/C} + C_{P,\text{SiO}/C}) + \mathcal{O}(\epsilon),$$

417 as leading order terms to equations (18) and (19). Combining these with the leading order terms in (16), and
 418 using $r = C_{\text{SiO}_2(\text{s})}(T - T_m)^+$ as the functional form for $r := r_3 = r_5$, we obtain the leading order equations,
 419 with $\mathcal{O}(\epsilon)$ corrections,

$$420 \quad (57) \quad \frac{\partial}{\partial t} \left(\left(\frac{T_{\text{top}}}{T_0} + T \right) (\sigma_s + \sigma_{gr}^*) \right) + \frac{\partial}{\partial z} \left(\left(\frac{T_{\text{top}}}{T_0} + T \right) \frac{U_g \sigma_g}{2} \right) \\ = a \frac{\partial T^2}{\partial z^2} + \beta^* \frac{\partial}{\partial z} \left(\left(\frac{T_{\text{top}}}{T_0} + T \right)^3 \frac{\partial T}{\partial z} \right) + \gamma_5 C_{\text{SiO}_2(\text{s})} (T - T_m)^+ + qF(z),$$

$$422 \quad (58) \quad \frac{\partial}{\partial z} (U_g C_g) = 2C_{\text{SiO}_2(\text{s})} (T - T_m)^+, \quad \frac{\partial C_{\text{SiO}_2(\text{s})}}{\partial t} = -C_{\text{SiO}_2(\text{s})} (T - T_m)^+,$$

$$424 \quad (59) \quad g_0 \left(T + \frac{T_{\text{top}}}{T_0} \right) C_g + C_{\text{SiO}_2(\text{s})} (m_C + m_{\text{SiO}_2(\text{s})}) + (1 - \alpha) m_C = 1,$$

425 along with boundary and initial conditions

$$426 \quad (60) \quad \frac{\partial T(0, t)}{\partial z} = 0 = \frac{\partial T(1, t)}{\partial z}, \quad T(z, 0) = T_a = -1.1, \quad U_g(0, t) = 0, \quad C_{\text{SiO}_2(\text{s})}(z, 0) = \alpha.$$

427 We further simplify our system by neglecting radiation, since $\beta^* \left(\frac{T_{top}}{T_0} + T \right)^3 / a \sim 0.27$ at the base, and
 428 thermal convection from (57). Although these are both order one effects, we seek to get the simplest model
 429 which represents the main physical and chemical effects, thus making the analysis more tractable. We thus
 430 replace (57) with

$$(61) \quad \frac{\partial}{\partial t} \left(\left(\frac{T_{top}}{T_0} + T \right) (C_{\text{SiO}_2(s)} (1 + C_{P,\text{SiO}_2(s)/C}) + (1 - \alpha) + \sigma_{gr}^*) \right) = a \frac{\partial T^2}{\partial z^2} + \gamma_5 C_{\text{SiO}_2(s)} (T - T_m)^+ + qF(z).$$

432 The gas flux equation, which is the first in (58), decouples and we are left with the system (61) and the
 433 second equation in (58) to be solved for the temperature and concentration of solid quartz. This is still quite
 434 complex, so we make an additional approximation. Since the model assumes a constant thermal conductivity,
 435 it is not unreasonable to replace the varying heat capacity with a constant heat capacity. We take this to
 436 be the average of the minimum and maximum values of the heat capacity, that is

$$(62) \quad \sigma = \frac{\alpha}{2} (1 + C_{P,\text{SiO}_2(s)/C}) + (1 - \alpha) + \sigma_{gr}^*.$$

438 We note that γ_5 is negative [21], so for clarity we use the notation $\gamma := -\gamma_5$. This give the system

$$(63) \quad \sigma \frac{\partial T}{\partial t} = a \frac{\partial T^2}{\partial z^2} - \gamma C_{\text{SiO}_2(s)} (T - T_m)^+ + qF(z), \quad \frac{\partial C_{\text{SiO}_2(s)}}{\partial t} = -C_{\text{SiO}_2(s)} (T - T_m)^+,$$

440

$$(64) \quad \frac{\partial T(0, t)}{\partial z} = 0 = \frac{\partial T(1, t)}{\partial z}, \quad T(z, 0) = T_a = -1.1, \quad C_{\text{SiO}_2(s)}(z, 0) = \alpha.$$

442 We have the furnace heating up from cold due to a wall source term $F(z)$, up to a time when the temperature
 443 reaches the melting point of quartz, T_m , in the base of the furnace. Then solid quartz melts to form liquid
 444 quartz, at a rate $r_3 = C_{\text{SiO}_2(s)} (T - T_m)^+$. This melting does not release any heat in our full model, but
 445 we have a reaction balance between the reactions r_3 and r_5 , in which carbon reacts with the newly formed
 446 liquid quartz to produce gaseous CO and SiO. This pair of reactions is highly endothermic, taking in heat
 447 from the surroundings. Thus, energy needs to be input from the walls in order for the carbon and quartz to
 448 react, but since this reaction is endothermic it slows down the rate of temperature increase.

449 In order to write this system in a cleaner mathematical form, we choose to rescale time to balance with
 450 the endothermic heat of reaction, so introduce the scalings

$$(65) \quad T = T_m + \hat{T}(T_m - T_a), \quad C_{\text{SiO}_2(s)} = \alpha \hat{C}, \quad t = \frac{\sigma}{\gamma \alpha} \hat{t}.$$

452 Dropping the hat notation we have the system

$$(66) \quad \frac{\partial T}{\partial t} = K \frac{\partial^2 T}{\partial z^2} - CT^+ + \omega F(z),$$

454

$$(67) \quad \frac{\partial C}{\partial t} = -bCT^+,$$

456 with initial and boundary conditions

$$(68) \quad T(z, 0) = -1, \quad C(z, 0) = 1, \quad \frac{\partial T(0, t)}{\partial z} = 0 = \frac{\partial T(1, t)}{\partial z}.$$

458 The three dimensionless parameters are written in terms of previous dimensionless parameters as

$$(69) \quad K = \frac{a}{\gamma \alpha}, \quad b = \frac{(T_m^* - T_a)\sigma}{\gamma \alpha}, \quad \omega = \frac{q}{(T_m^* - T_a)\gamma \alpha}.$$

460 Typical parameter sizes are $K = 0.01$, $b = 0.3$, and $\omega = 0.15$. We will use these values throughout
461 this section unless otherwise stated. In Figure 6 we show plots comparing the numerical solutions of this
462 simplified system with the full system presented in Section 1. In the full system heat equation (16) the heat
463 capacity can vary, so in order for a fair comparison we restrict the heat capacity in the time derivative of
464 the full numerics to be the constant σ from (62). We could alternatively have kept a varying heat capacity
465 in the simplified system, but this would make the asymptotic analysis more difficult. The heat capacity of
466 the gas in the spatial derivative of (16) is still allowed to vary, since this is not included in the simplified
467 model. The temperatures of the two systems match well for the first 40 mins in the base of the furnace,
468 but the simplified numerics become hotter in the base after this. This is because thermal convection and
469 radiation, which transfer heat from the base to the top of the furnace, are present in the full model, but not
470 in the simplified model. The effect of this is to produce more $\text{SiO}_2(\text{s})$ in the base in the simplified model.
471 Also, the exothermic heat sources from reactions r_1 and r_2 are present in the full model only, adding to
472 the discrepancy of the temperature in the upper furnace. However, despite these differences, the overall
473 qualitative behaviour is similar between the two models. We have the base of the furnace heating up faster
474 than the top and, upon reaching a critical temperature, solid quartz melting then reacting to form gas. It
475 is thus instructive to consider this simplified model to develop understanding as to the qualitative effects in
476 the pilot furnace.

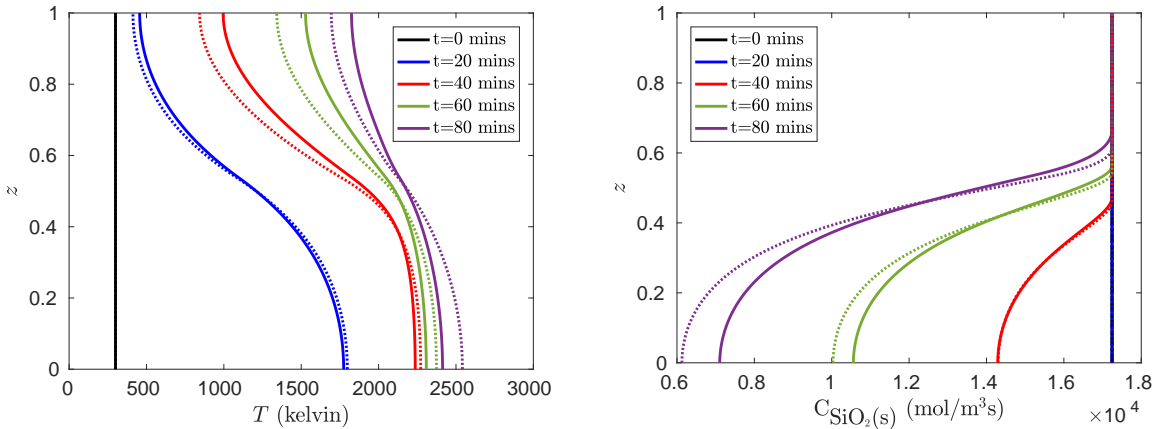


Fig. 6: Comparison of numerics of the full system (11), (14) - (20) (with a constant heat capacity) in solid lines and numerics for the simplified system (66) - (68) in dotted lines. On the left are plots of temperature and on the rights are plots of $C_{\text{SiO}_2(\text{s})}$ (both dimensional). Parameter values used are $\epsilon = 0.16$, $\delta = 3.2 \times 10^{-4}$, and $\alpha = 0.45$.

477 **4.1. Early time.** For early time the temperature is not hot enough for the reaction to take place,
478 meaning no energy is consumed by the reaction. Taking the heat source from the wall to be the step
479 function $F(z) = \mathcal{H}(h_T^* - z)$ in this case, for ease of analysis, we have

$$480 \quad (70) \quad \frac{\partial T}{\partial t} = K \frac{\partial^2 T}{\partial z^2} + \omega \mathcal{H}(h_T^* - z),$$

481 with initial condition and boundary conditions

$$482 \quad (71) \quad T(z, 0) = -1, \quad \frac{\partial T(0, t)}{\partial z} = \frac{\partial T(1, t)}{\partial z} = 0.$$

483 We can find a series solution to this problem as

$$484 \quad (72) \quad T(z, t) = T_a + \omega h_T^* t + \frac{2\omega}{K} \sum_{n=1}^{\infty} \frac{\sin(n\pi h_T^*)}{n^3 \pi^3} (1 - \exp(-Kn^2 \pi^2 t)) \cos(n\pi z).$$

485 In Figure 7 we compare this solution to numerics of the system (66) - (68). There is good agreement in
 486 the early time pre-heating region, then the solutions diverge when $T > 0$, where the endothermic reaction
 occurs.

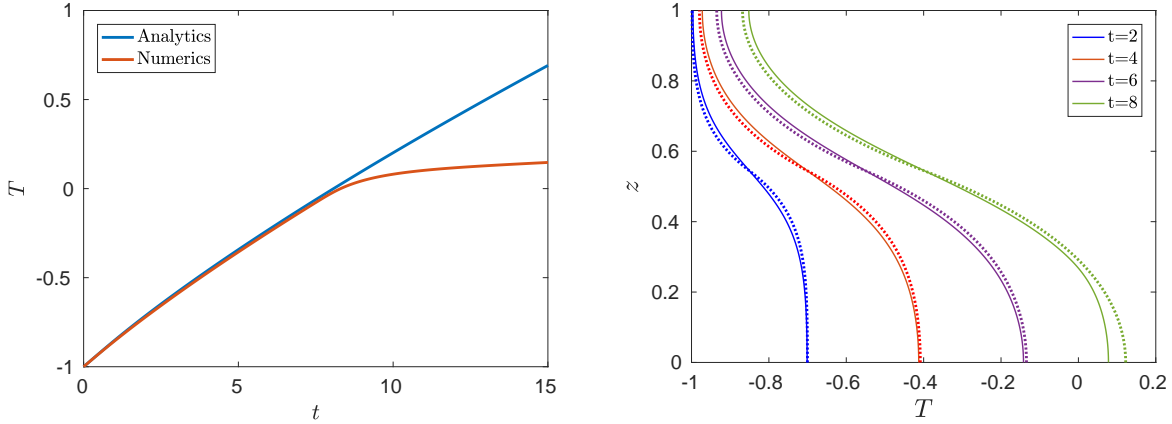


Fig. 7: Comparison of analytical solution (72) with numerics. On the left is the dimensionless temperature for fixed height $z = 0.3$ and on the right are spatial profiles at different times, with the analytic solution in dotted lines and numerics in solid lines.

487

488 **4.2. Small diffusion limit.** In Figure 8 we show contour plots for T and C for the cases $K = 0.01$
 489 and $K = 0$, with $b = 0.3$ and $\omega = 0.15$ in each case. When there is no diffusion, so $K = 0$, we see a
 490 sharp interface between a pre-heating region in the upper-left of the (z, t) -plane and a reaction zone in
 491 the lower-right of the plane. Throughout this section and Section 4.3 we use the smooth heating function
 492 $F(z) = \frac{1}{2}(1 + \tanh(10(h_T^* - z)))$, with $h_T^* = 0.544$, in numerical simulations and asymptotic solutions shown
 493 in figures.

494 A schematic of the two regions is given in Figure 9. Region A is the pre-heating region, where the
 495 temperature is too cold for the reaction to take place. In Region B the temperature is positive, so the
 496 chemical reacts. Let $z = s(t)$ be defined as the interface between these regions. We plot numerical solutions
 497 for a fixed height $z = 0.3$ in Figure 10, indicating where these regions occur. A third region, Region C,
 498 where all the chemical is nearly used up and the temperature increases linearly in the graphite crucible due
 499 to the heat source from the wall. We are not interested in Region C in this paper, since it corresponds to
 500 all the solid material being used up in the furnace, and the pilot furnace experiments do not run for long
 501 enough for this to be observed. Unlike the sharp interface between Regions A and B at $z = s(t)$ (shown by
 502 the dashed line), there is no sharp interface between Regions B and C, however we have put an interface in
 503 (shown by the dot-dashed line) to illustrate a possible location to distinguish between the regions.

504 Our model has the small parameter K . We treat ω and b as order one constants and expand in terms of
 505 K , with $0 < K \ll 1$, so that we write $T^{A/B} = T_0^{A/B} + KT_1^{A/B} + \mathcal{O}(K^2)$, $C^{A/B} = C_0^{A/B} + KC_1^{A/B} + \mathcal{O}(K^2)$,
 506 and $s(t) = s_0(t) + Ks_1(t) + \mathcal{O}(K^2)$, where $T^{A/B}$ and $C^{A/B}$ refer to T and C in Regions A and B respectively.
 507 The first order equations correspond to the limit of zero diffusion. In this case, the spatial dependency for
 508 the problem comes through the general heating source term $F(z)$, which we take to be order one and hotter
 509 at the base than at the top.

510 In Region A we have the following system at leading order,

$$511 \quad (73) \quad \frac{\partial T_0^A}{\partial t} = \omega F(z) + \mathcal{O}(K), \quad \frac{\partial C_0^A}{\partial t} = \mathcal{O}(K), \quad T_0^A(z, 0) = -1 + \mathcal{O}(K), \quad C_0^A(z, 0) = 1 + \mathcal{O}(K),$$

512 which has the solution

$$513 \quad (74) \quad T_0^A(z, t) = -1 + \omega F(z)t, \quad C_0^A(z, t) = 1.$$

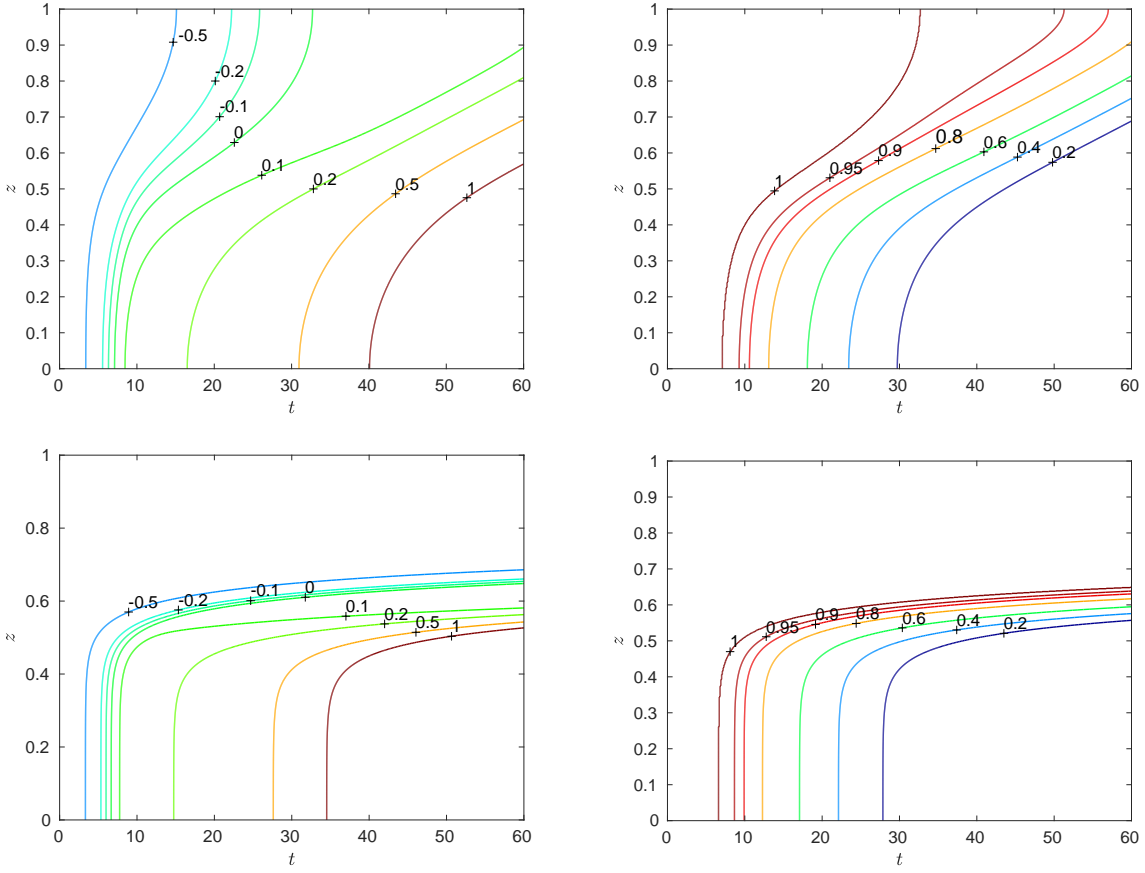


Fig. 8: Contour plots for dimensionless T (left) and C (right), in the cases $K = 0.01$ (top) and $K = 0$ (bottom), with $b = 0.3$ and $\omega = 0.15$ in all cases.

514 We find that $C^A \equiv 1$, and that the higher order equations for temperature are given by

515 (75)
$$\frac{\partial T_n^A}{\partial t} = \frac{\partial^2 T_{n-1}^A}{\partial z^2}, \quad n \geq 1.$$

516 Thus we have the following expansion in K for temperature in Region A

517 (76)
$$T^A(z, t) = -1 + \omega F(z)t + \omega \sum_{n=1}^{\infty} K^n F^{(2n)}(z) \frac{t^{n+1}}{(n+1)!}.$$

518 To find the coefficients in the expansion of $s(t)$ we note that the curve $z = s(t)$ is given by

519 (77)
$$T^A(s(t), t) = 0.$$

520 Hence

521 (78)
$$\begin{aligned} 0 &= T^A(s_0(t) + Ks_1(t) + \dots, t) \\ &= T^A(s_0(t), t) + (Ks_1(t) + \dots) \frac{\partial T^A}{\partial z}(s_0(t), t) + \dots \\ &= T_0^A(s_0(t), t) + K \left(T_1^A(s_0(t), t) + s_1(t) \frac{\partial T_0^A}{\partial z}(s_0(t), t) \right) \\ &\quad + K^2 \left(T_2^A(s_0(t), t) + s_1(t) \frac{\partial T_1^A}{\partial z}(s_0(t), t) + s_2(t) \frac{\partial T_0^A}{\partial z}(s_0(t), t) + \frac{1}{2} s_1(t)^2 \frac{\partial^2 T_0^A}{\partial z^2}(s_0(t), t) \right) + \mathcal{O}(K^3). \end{aligned}$$

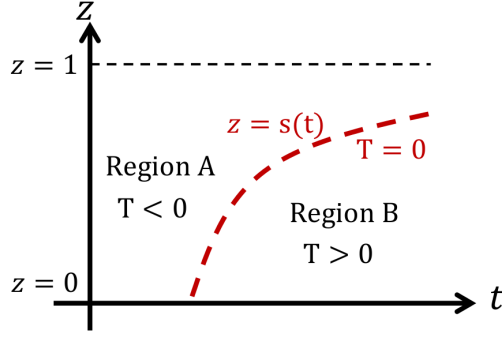


Fig. 9: Schematic of the different regions in the variable temperature problem. In Region A the temperature is too cold for the reaction to take place, whilst in Region B the chemical reacts. These regions are separated by the interface $z = s(t)$, given by the isotherm $T = 0$.

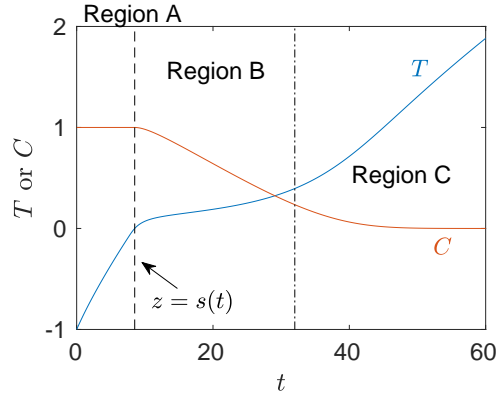


Fig. 10: Numerical simulations of dimensionless T and C from the system (66) - (68), displayed for fixed height $z = 0.3$. Region A is to the left of the dashed line, Region B is between the dashed and the dot-dashed lines, and Region C is to the right of the dot-dashed line. The dashed line has label $z = s(t)$, because it is showing the time for which there is a transition between Regions A and B for the given height $z = 0.3$. The dot-dashed line is in a possible, illustrative location. Parameter values used are $K = 0.01$, $\omega = 0.15$, and $b = 0.3$.

522 Looking at leading order we get

523 (79)
$$\mathcal{O}(1) : s_0(t) = F^{-1} \left(\frac{1}{\omega t} \right),$$

524 which requires that F be invertible. At next order we get

525 (80)
$$\mathcal{O}(K) : s_1(t) = -\frac{1}{2} \frac{F''(s_0(t))}{F'(s_0(t))} t,$$

526 and then looking at terms quadratic in K we find

527 (81)
$$\mathcal{O}(K^2) : s_2(t) = \left(\frac{F''(s_0(t))F'''(s_0(t))}{4(F'(s_0(t)))^2} - \frac{F^{IV}(s_0(t))}{6F'(s_0(t))} - \frac{(F''(s_0(t)))^3}{8(F'(s_0(t)))^3} \right) t^2.$$

528 This iterative process can be continued to find the correction for $s(t)$ to any order of K , if desired.

529 In Region B we have obtained the leading order equations,

530 (82)
$$\frac{\partial T_0^B}{\partial t} = -C_0^B T_0^B + \omega F(z) + \mathcal{O}(K), \quad \frac{\partial C_0^B}{\partial t} = -b C_0^B T_0^B + \mathcal{O}(K),$$

531 with the boundary conditions

532 (83)
$$T_0^B(s_0(t), t) = \mathcal{O}(K), \quad C_0^B(s_0(t), t) = 1 + \mathcal{O}(K),$$

533 which we can write as

534 (84)
$$T_0^B = 0 \quad \text{and} \quad C_0^B = 1 \quad \text{on} \quad t = \frac{1}{\omega F(z)}.$$

535 We can write the equations in (82) as

536 (85)
$$\frac{\partial}{\partial t} \left(T_0^B - \frac{1}{b} C_0^B \right) = \omega F(z), \quad \frac{\partial C_0^B}{\partial t} = -b C_0^B T_0^B.$$

537 Integrating the first equation we get the relation

538 (86)
$$T_0^B = \frac{1}{b} (C_0^B - 1) - 1 + \omega F(z)t,$$

539 which can be substituted into the second equation to get the ODE

540 (87)
$$\frac{\partial C_0^B}{\partial t} = -(C_0^B)^2 + C_0^B (1 + b - b\omega F(z)t).$$

541 Equation (87), along with the boundary condition in (84), has the solution

542 (88)
$$C_0^B(z, t) = \frac{\exp\left(-\frac{2+b}{2\omega F(z)} + (b+1)t - \frac{b\omega F(z)}{2}t^2\right)}{1 + \sqrt{\frac{\pi}{2b\omega F(z)}} \exp\left(\frac{1}{2b\omega F(z)}\right) \left[\operatorname{erf}\left(\frac{1}{\sqrt{2b\omega F(z)}}\right) + \operatorname{erf}\left(\frac{b\omega F(z)t - b - 1}{\sqrt{2b\omega F(z)}}\right) \right]},$$

543 and hence the temperature is given by

544 (89)
$$T_0^B(z, t) = -1 - \frac{1}{b} + \omega F(z)t + \frac{\exp\left(-\frac{2+b}{2\omega F(z)} + (b+1)t - \frac{b\omega F(z)}{2}t^2\right)}{b + \sqrt{\frac{\pi b}{2\omega F(z)}} \exp\left(\frac{1}{2b\omega F(z)}\right) \left[\operatorname{erf}\left(\frac{1}{\sqrt{2b\omega F(z)}}\right) + \operatorname{erf}\left(\frac{b\omega F(z)t - b - 1}{\sqrt{2b\omega F(z)}}\right) \right]}.$$

545 The $\mathcal{O}(K)$ equations are solvable, but require tedious calculations, especially to determine the required $\frac{\partial^2 T_0^B}{\partial z^2}$,
 546 so we do not include the functional form of solutions here, but instead give solutions in integral form in the
 547 appendix.

548 In Figure 11 we compare the leading order asymptotic solutions with the numerical results of the sim-
 549 plified system, at a fixed height in the bottom of the furnace. In Figure 12 we show spatial comparisons for
 550 different fixed times. We see that the first order asymptotics capture the main behaviour of the numerics at
 551 the base, but are off by a small error, which we expect would be corrected by finding higher order terms to
 552 account for the role of thermal diffusion. The temperature at the top of the furnace is not captured by the
 553 leading order asymptotics, since this does not include diffusion and the chosen heat source is close to zero
 554 here.

555 **4.3. Small heating limit.** We can also consider the case where ω is also a small parameter, with
 556 $0 < K \ll \omega \ll 1$. Here the heat absorbed by the endothermic reaction between the melted quartz and
 557 the carbon is larger than the heat input from the electrode or the induction furnace, but the heat transfer
 558 from this source term dominates over diffusion as the main heating mechanism. Asymptotic analysis can be
 559 performed with $K = \mathcal{O}(\omega^2)$ and considering the limit $\omega \rightarrow 0$. We will not give the details of this analysis
 560 here, but find similar behaviour in Region A to that discussed in the small diffusion limit in Section 4.2.

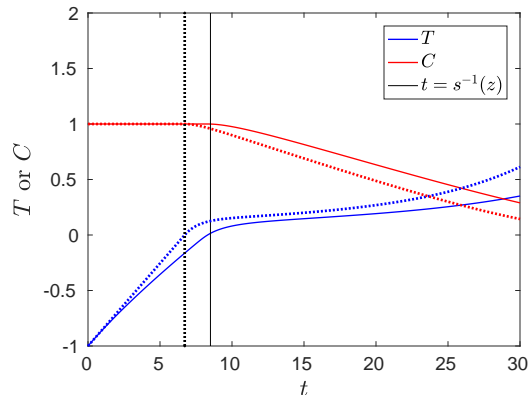


Fig. 11: Comparison of first order asymptotics, shown in dotted lines, and numerics of the simplified system (66) - (68), shown in solid lines, at height $z = 0.3$ for the dimensionless temperature, concentration, and time taken to reach the interface between Regions A and B. Parameter values used are $K = 0.01$, $\omega = 0.15$, and $b = 0.3$.

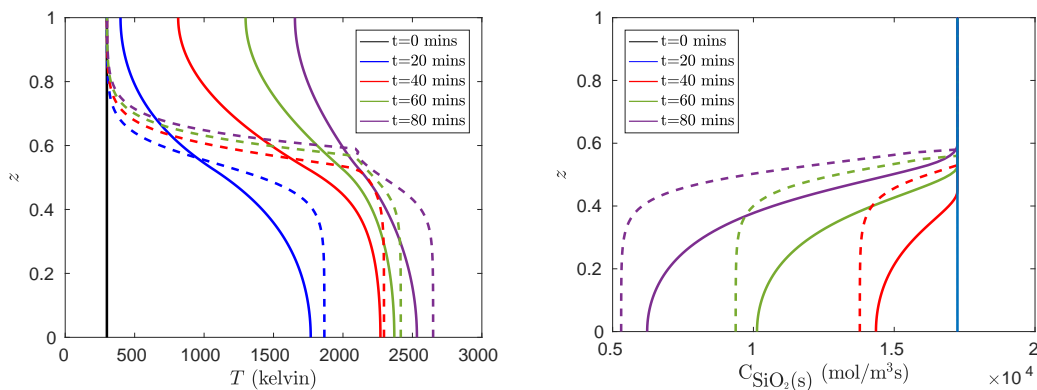


Fig. 12: Comparison of asymptotics, shown in dotted lines, and numerics of the simplified system (66) - (68), shown in solid lines, for the dimensional temperature (left) and concentration (right). Since the smooth heating source was used the simplified numerics are different than those in Figure 6, which use a Heaviside function. Parameter values used are $K = 0.01$, $\omega = 0.15$, and $b = 0.3$.

561 The chemical C remains unreacted and the temperature increases due to the heat source $F(z)$, with spatial
562 variation again coming in from derivatives of $F(z)$. The interface $z = s(t)$ can be determined using the same
563 method employed to find (79) - (81), and similar functional forms are found, with the leading order location
564 of the interface being given by the heat source $F(z)$. In Region B the concentration reacts away, with the
565 $\mathcal{O}(1)$ changes found being larger than the $\mathcal{O}(\omega)$ changes in temperature. Since the temperature is small, the
566 dominant balance is between the heating and the endothermic reaction. Thus the whole problem is heat
567 controlled and the temperature in the furnace changes to balance the energy input. However, the leading
568 order solution for temperature in Region B blows up in finite time, as temperature changes increase. This
569 issue does not occur in the small diffusion limit in Section 4.2, where ω is treated as an $\mathcal{O}(1)$ parameter.

570 By considering the full model we have reduced the number of equations to a simplified system, which
571 captures the coupled evolution of temperature and concentration of solid quartz in the furnace. This model
572 has two regions of interest; the pre-heating Region A and the reaction zone Region B. An analytic series
573 solution was found for Region A and the simplified model was considered in the limit of small diffusion, and a
574 small heat source. When diffusion is small, the location of interface between Regions A and B is determined

575 to leading order by the functional form of the heating source. When the parameter ω is also considered to
576 be small, then the temperature is small in Region B, and the main balance in the problem is between the
577 energy input from the induction furnace and the energy absorbed by the endothermic reaction. Numerical
578 simulations of the simplified model compare well with the full model, so that the simplifications discussed
579 will be useful for future models.

580 **5. Crust formation.** We are particularly interested in furnace crust formation, since this slows down
581 the industrial operation and requires ‘stoking’. General insights into this crust can be found from the reaction
582 pathways in (1) - (5), with additional understanding from the analysis of the dimensionless equations with
583 prescribed temperature profile in Section 3 and the full model in Section 4.

584 The composition of furnace crust is not well-understood [18], and so as a proxy we consider the volume
585 fraction of solid and liquid material, from here on called the solid volume fraction θ_S . This is discussed in
586 more detail in [21]. Note that liquid quartz is highly viscous and can clog up pores in the furnace. Although
587 liquid silicon is less viscous, we include it in the definition for simplicity. We can look at whether the time
588 rate of change of θ_S is positive or negative in the upper part of the furnace, to determine if crust is building
589 up. θ_S is defined as

$$590 \quad (90) \quad \theta_S = \sum_{\text{solids and liquids } i} \frac{M_i}{\rho_i} C_i,$$

591 for dimensional C_i , so taking a time derivative we can substitute in the reaction rates from the matrix (6).
592 We can make progress even if we do not define functional forms of the reaction rates or the associated
593 parameter values. This is helpful, since you can still study crust formation regardless of the functional forms
594 chosen. We thus refer to the rates as R_j , as described in (1) - (5). Note that these are dimensional variables.
595 In the upper part of the furnace, where the temperature is too cold for quartz to melt, we impose $R_3 = 0$ to
596 get

$$597 \quad (91) \quad \frac{\partial \theta_S}{\partial t} = \frac{M_C}{\rho_C} (-2R_1 - R_5) + \frac{M_{\text{SiC}}}{\rho_{\text{SiC}}} (R_1 - R_4) + \frac{M_{\text{SiO}_2(l)}}{\rho_{\text{SiO}_2(l)}} (R_2 - R_{-2} - R_5) + \frac{M_{\text{Si}}}{\rho_{\text{Si}}} (R_2 - R_{-2} - R_4).$$

598 In the top of the furnace carbon reacts with the available $\text{SiO}_2(l)$, which is produced from the condensation
599 reaction R_2 . Since we expect quantities of Si and $\text{SiO}_2(l)$ to be small compared to the amount of carbon,
600 we can write $R_{-2} \ll R_5$ and $R_5 = R_2$. If we further assume a functional dependence of R_4 on $(P - P_4)^+$,
601 as done in (9), then $R_4 = 0$ in the upper part of the furnace, because the partial pressure of SiO is too low.
602 With these assumptions, we can simplify equation (91) to

$$603 \quad (92) \quad \frac{\partial \theta_S}{\partial t} = \left(\frac{M_{\text{SiC}}}{\rho_{\text{SiC}}} - 2 \frac{M_C}{\rho_C} \right) R_1 + \left(\frac{M_{\text{Si}}}{\rho_{\text{Si}}} - \frac{M_C}{\rho_C} \right) R_2.$$

604 The molar masses are known constants and can be found from [14]. We take the density of carbon, silicon
605 carbide, and silicon from [10], [15], and [9] respectively. With this data, we have

$$606 \quad (93) \quad \frac{M_C}{\rho_C} = 5.298 \times 10^{-6}, \quad \frac{M_{\text{SiC}}}{\rho_{\text{SiC}}} = 1.249 \times 10^{-5}, \quad \frac{M_{\text{Si}}}{\rho_{\text{Si}}} = 1.206 \times 10^{-5}.$$

607 This means that $\frac{\partial \theta_S}{\partial t} > 0$, and as such we will see a build up of solid in our model. This corresponds in turn
608 to crust formation, regardless of the functional form of reaction rates R_1 , R_2 , and R_5 , and regardless of how
609 large the kinetic parameters are. Notice though that the sign of $\frac{M_{\text{SiC}}}{\rho_{\text{SiC}}} - 2 \frac{M_C}{\rho_C}$ is quite sensitive to the data
610 used in [9] and [10]. A decrease in the value of ρ_C by 15% or an increase in the value of ρ_{SiC} by 18% would
611 change the sign, and it would not then be true that solid always builds up.

612 We can also incorporate the solutions from Section 3, with a prescribed temperature profile $T(z)$. With
613 these we find

$$614 \quad (94) \quad \theta_S = m_C + \alpha m_{\text{SiO}_2(s)} + \epsilon \left[\chi_1 \left(\frac{1}{2} - P_1 \right) (m_{\text{SiC}} - 2m_C) + \chi_2 \left(\frac{1}{2} - P_2 \right) (m_{\text{Si}} - m_C) \right] t + \mathcal{O}(\epsilon^2),$$

615 and so can quantify how the crust grows. Taking a spatial partial derivative and using the chain rule, we see

616 (95)
$$\frac{\partial\theta_S}{\partial z} = -\epsilon \left[\chi_1 \frac{dP_1}{dT} (m_{\text{SiC}} - 2m_C) + \chi_2 \frac{dP_2}{dT} (m_{\text{Si}} - m_C) \right] \frac{dT}{dz} t + \mathcal{O}(\epsilon^2).$$

617 Since $\frac{dP_1}{dT}, \frac{dP_2}{dT} > 0$ (see the equilibrium partial pressures figure in [18]) and $\frac{dT}{dz} < 0$ (because of the temper-
618 ature gradient in the furnace) then

619 (96)
$$\frac{\partial\theta_S}{\partial z} > 0.$$

620 Hence, the solid volume fraction increases with height in the furnace, according to this model, and the charge
621 is most porous at the lower interface with the gas cavity.

622 In Section 4 the analysis did not consider solid build-up in the upper furnace, since this is an $\mathcal{O}(\epsilon)$
623 effect when compared to the $\mathcal{O}(1)$ changes taking place in the lower, hotter region. However, we tracked the
624 location of the interface at the base of the charge through the isotherm $T = 0$ (or $T=1996$ K in dimensional
625 units). This position is largely driven by the external heat source, since diffusion effects are small. Since
626 temperature remains monotone throughout, assuming a monotone heat source F , then to leading order r_1
627 and r_2 increase with furnace height and thus the rate of crust increase in (92) will increase as well.

628 **6. Discussion.** We have investigated asymptotic limits of the silicon furnace model developed in [21],
629 extending the analysis that was undertaken through numerical simulations in that paper. Natural small
630 parameters are the ratio of the timescale for the reaction between carbon and liquid quartz to the timescale
631 for the melting of quartz, and the ratio of timescale of gas advection to the timescale of the melting of
632 quartz. With appropriate scalings for the concentrations we have been able to determine the leading order
633 chemical behaviour for different spatial regions in the furnace, when a prescribed temperature is imposed
634 in the model. In Region II we find the dominant behaviour is solid quartz melting to liquid quartz, which then
635 reacts with the available carbon particles to form gaseous CO and SiO. In Region I this SiO gas condenses
636 into silicon and liquid quartz, and also reacts with carbon to form silicon carbide and CO. This competition
637 between reactions, determining how much SiC and Si is produced, is represented in the size of the parameter
638 $\lambda = \chi_2/\chi_1$. We have also been able to capture early time behaviour in these regions, where the variables
639 move from the initial conditions to typical furnace behaviour.

640 In Section 4 we considered asymptotics of the full model with temperature allowed to vary in time.
641 Through systematic reductions we have derived a simplified system of two coupled equations for temperature
642 and the concentration of solid quartz, which depends on three parameters, ten times fewer than the number
643 used in the full model. These three parameters represent the heating from the external source, the thermal
644 diffusion, and the rate of melting of solid quartz. Numerical simulations of the simplified system compare well
645 the full model, showing the same qualitative behaviour. We find asymptotic solutions to the reduced system,
646 treating the diffusivity, K , as a small parameter. The leading order solutions, where no diffusion occurs,
647 are representative of the behaviour in the reaction zone. This suggests that the dominant heat transfer
648 mechanisms are the energy input from the induction furnace into the pilot furnace, and the heat absorption
649 of the endothermic reaction between carbon and quartz. The pilot furnace is most thermally conductive
650 along the graphite walls, since conduction between solid particles is relatively small. In an industrial furnace
651 the subdominance of diffusion is likely to be even more pronounced, since energy is input directly from the
652 electrodes.

653 By examining crust formation in Section 5, we found crust builds up in this model regardless of the
654 functional forms or kinetic parameters of reaction rates R_1 and R_2 . However, the model assumes that there
655 is no solid or liquid motion and that everywhere in the furnace there is a mixture of solid, liquid, and gas. In
656 practice liquid silicon is inviscid, and so will drip to the crater when produced. This would have an impact on
657 crust formation, as silicon would not contribute to the solid fraction in the upper furnace, as it does in (92).
658 In addition, the porosity will become so low at the bottom of the charge that solid and liquid material will
659 fall to the furnace base. Clearly there needs to be a failure criterion for this falling material. One possibility
660 is to use the melting isotherm, so that all material hotter than this will have fallen to the base. The reduced
661 system in Section 4 will be useful when further physical effects are incorporated in future models, such as
662 the dripping of inviscid silicon, the falling of material from the charge to the crater, and the two dimensional
663 mechanical bridging of the crust.

664 **Appendix: Asymptotic Expansions.** Here we list asymptotic solutions to leading and first order,
665 for each sub-problem considered. For simplicity in the prescribed temperature asymptotics we expand the
666 gas flux as one variable, so that $U_g C_g = U_g^0 C_g^0 + \epsilon U_g^1 C_g^1 + \mathcal{O}(\epsilon^2)$. If instead we used individual expansions
667 $U_g = U_g^0 + \epsilon U_g^1 + \mathcal{O}(\epsilon^2)$, $C_g = C_g^0 + \epsilon C_g^1 + \mathcal{O}(\epsilon^2)$ then the leading order asymptotics remain the same, but there
668 will be more complex relationships for the first order terms, which include the algebraic no voids condition.
669 For brevity we suppress the notation $T(z)$ and $P_i(T(z))$ to T and P_i respectively, unless we are integrating
670 over a dummy variable.

671 **Prescribed Temperature - Region IIa.** On the early timescale $\hat{t} = t/\epsilon$ the solid and liquid concen-
672 trations are given by

$$673 \quad (97) \quad C_C = 1 + \epsilon \alpha (T - T_m) (\hat{t} + e^{-\hat{t}} - 1) + \mathcal{O}(\epsilon^2),$$

674

$$675 \quad (98) \quad C_{SiC} = \epsilon \chi_1 \left(\frac{1}{2} - P_1 \right) \hat{t} + \mathcal{O}(\epsilon^2),$$

676

$$677 \quad (99) \quad C_{SiO_2(s)} = \alpha - \epsilon \alpha (T - T_m) \hat{t} + \mathcal{O}(\epsilon^2),$$

678

$$679 \quad (100) \quad C_{SiO_2(l)} = \alpha (T - T_m) (1 - e^{-\hat{t}}) + \epsilon \left(\chi_2 \left(\frac{1}{2} - P_2 \right)^+ (1 - e^{-\hat{t}}) - \alpha (T - T_m)^2 (\hat{t} - 1 + e^{-\hat{t}}) \right. \\ \left. - \alpha^2 (T - T_m)^2 \left(\hat{t} - 2 + e^{-\hat{t}} \left(-\frac{\hat{t}^2}{2} + 2\hat{t} + 1 \right) + e^{-2\hat{t}} \right) \right) + \mathcal{O}(\epsilon^2),$$

680

$$681 \quad (101) \quad C_{Si} = \epsilon \chi_2 \left(\frac{1}{2} - P_2 \right)^+ \hat{t} + \mathcal{O}(\epsilon^2).$$

682 The gas flux and partial pressure are found to be

$$683 \quad (102) \quad U_g C_g = 2\alpha (1 - e^{-\hat{t}}) \int_{y=0}^{y=z} (T(y) - T_m) dy + 2\epsilon \int_{y=0}^{y=z} r_{5,IIa}^1(\hat{t}, y) - r_{2,IIa}^0(\hat{t}, y) dy + \mathcal{O}(\epsilon^2),$$

684

$$685 \quad (103) \quad P = \frac{1}{2} - \epsilon \frac{\int_{y=0}^{y=z} r_{1,IIa}^0(\hat{t}, y) + r_{2,IIa}^0(\hat{t}, y) dy}{U_g^0 C_g^0} + \mathcal{O}(\epsilon^2), \quad \text{for } U_g^0 C_g^0 \neq 0, \text{ i.e. } \hat{t}, z > 0,$$

686 where $U_g^0 C_g^0$ is the leading term in (102), and

$$687 \quad (104) \quad r_{1,IIa}^0(\hat{t}, z) = \chi_1 \left(\frac{1}{2} - P_1 \right), \quad r_{2,IIa}^0 = \chi_2 \left(\frac{1}{2} - P_2 \right)^+,$$

688

$$689 \quad (105) \quad r_{5,IIa}^1 = \alpha^2 (T - T_m)^2 (\hat{t} + e^{-\hat{t}} - 1) (1 - e^{-\hat{t}}) + \left(\chi_2 \left(\frac{1}{2} - P_2 \right)^+ (1 - e^{-\hat{t}}) \right. \\ \left. - \alpha (T - T_m)^2 (\hat{t} - 1 + e^{-\hat{t}}) - \alpha^2 (T - T_m)^2 \left(\hat{t} - 2 + e^{-\hat{t}} \left(-\frac{\hat{t}^2}{2} + 2\hat{t} + 1 \right) + e^{-2\hat{t}} \right) \right).$$

690 **Prescribed Temperature - Region IIb.** Since several of the higher order terms in this region can
691 only be written in terms of integrals, we give the $\mathcal{O}(1)$ terms and then the $\mathcal{O}(\epsilon)$ terms. Note that

$$692 \quad (106) \quad C_{\text{SiO}_2(\text{s})} = \alpha e^{-(T-T_m)t},$$

693 and so there is no correction term needed for the concentration of solid quartz. Five of the leading order
694 variables are easily found as

$$695 \quad (107) \quad C_{\text{C}}^0 = \alpha e^{-(T-T_m)t} + (1 - \alpha),$$

696

$$697 \quad (108) \quad C_{\text{SiO}_2(\text{l})}^0 = \frac{(T - T_m)\alpha e^{-(T-T_m)t}}{\alpha e^{-(T-T_m)t} + (1 - \alpha)},$$

698

$$699 \quad (109) \quad C_{\text{SiO}_2(\text{s})}^0 = \alpha e^{-(T-T_m)t},$$

700

$$701 \quad (110) \quad U_g^0 C_g^0 = 2\alpha \int_{y=0}^{y=z} e^{-(T(y)-T_m)t} (T(y) - T_m) dy,$$

702

$$703 \quad (111) \quad P^0 = \frac{1}{2}.$$

704 The solutions for C_{SiC}^0 and C_{Si}^0 are different in the temperature regions $P_2, P_4 \geq \frac{1}{2}$, $P_2 < \frac{1}{2} \leq P_4$, and
705 $P_4 < \frac{1}{2} \leq P_2$. Note that there is no region in $T > T_m$ where P_2 and P_4 are both less than $\frac{1}{2}$

706 In $P_2 < \frac{1}{2} \leq P_4$ we have

$$707 \quad (112) \quad C_{\text{SiC}}^0 = \chi_1 \left(\frac{1}{2} - P_1 \right) \left(\frac{\alpha}{T - T_m} \left(1 - e^{-(T-T_m)t} \right) + (1 - \alpha)t \right),$$

708

$$709 \quad (113) \quad C_{\text{Si}}^0 = \chi_2 \left(\frac{1}{2} - P_2 \right) \left(\alpha e^{-(T-T_m)t} + (1 - \alpha) \right)^{\chi_2 - 2} \int_{\tilde{t}=0}^{t=\tilde{t}} \left(\alpha e^{-(T-T_m)\tilde{t}} + (1 - \alpha) \right)^{-\chi_2} d\tilde{t}.$$

710 In $P_2, P_4 \geq \frac{1}{2}$ we have that C_{SiC}^0 is given by (112) and that $C_{\text{Si}}^0 = 0$. In $P_4 < \frac{1}{2} \leq P_2$

(114)

$$711 \quad C_{\text{SiC}}^0 = \begin{cases} \chi_1 \left(\frac{1}{2} - P_1 \right) \left[\frac{\alpha(e^{-(T-T_m)t} - e^{-\chi_4(\frac{1}{2}-P_4)t})}{\chi_4(\frac{1}{2}-P_4) - (T-T_m)} + \frac{1-\alpha}{\chi_4(\frac{1}{2}-P_4)} \left(1 - e^{-\chi_4(\frac{1}{2}-P_4)t} \right) \right], & \chi_4(\frac{1}{2} - P_4) \neq (T - T_m), \\ \chi_1 \left(\frac{1}{2} - P_1 \right) \left[\alpha t + \frac{1-\alpha}{\chi_4(\frac{1}{2}-P_4)} \left(1 - e^{-\chi_4(\frac{1}{2}-P_4)t} \right) \right], & \chi_4(\frac{1}{2} - P_4) = (T - T_m), \end{cases}$$

712

$$713 \quad (115) \quad C_{\text{Si}}^0 = 2\chi_4 \left(\frac{1}{2} - P_4 \right) \left(\alpha e^{-(T-T_m)t} + (1 - \alpha) \right)^{\chi_4 - 2} \int_{\tilde{t}=0}^{t=\tilde{t}} \frac{C_{\text{SiC}}^0(\tilde{t}, z)}{\left(\alpha e^{-(T-T_m)\tilde{t}} + (1 - \alpha) \right)^{\chi_4 - 2}} d\tilde{t}.$$

714 To find C_{C}^1 we note that

$$715 \quad (116) \quad \frac{\partial C_{\text{C}}^1}{\partial t} = \frac{\partial C_{\text{SiO}_2(\text{l})}^0}{\partial t} - 2r_1^0 - r_2^0 - r_{-2}^0,$$

716 which we can integrate to give

$$717 \quad (117) \quad C_{\text{C}}^1 = C_{\text{SiO}_2(\text{l})}^0 - (T - T_m)\alpha - \chi_2 \left(\frac{1}{2} - P_2 \right) t + \int_{\tilde{t}=0}^{\tilde{t}=t} -2C_{\text{C}}^0(\tilde{t}, z) \left(\frac{1}{2} - P_1 \right) + \chi_{-2} C_{\text{SiO}_2(\text{l})}^0(\tilde{t}, z) C_{\text{Si}}^0(\tilde{t}, z) d\tilde{t}.$$

718 The other $\mathcal{O}(\epsilon)$ terms are found to be

$$719 \quad (118) \quad C_{\text{SiO}_2(l)}^1 = \frac{1}{C_C^0} \left(\frac{\alpha(1-\alpha)(T-T_m)^2 e^{(T-T_m)t}}{(\alpha+(1-\alpha)e^{(T-T_m)t})^2} + \chi_2 \left(\frac{1}{2} - P_2 \right)^+ - \chi_{-2} C_{\text{SiO}_2(l)}^0 C_{\text{Si}}^0 - C_{\text{SiO}_2(l)}^0 C_C^1 \right),$$

720

$$721 \quad (119) \quad U_g^1 C_g^1 = 2 \int_{y=0}^{y=z} \left[C_{\text{SiO}_2(l)}^1(t, y) C_C^0(t, y) + C_{\text{SiO}_2(l)}^0(t, y) C_C^1(t, y) - \chi_2 \left(\frac{1}{2} - P_2 \right)^+ \right. \\ \left. + \chi_{-2} C_{\text{SiO}_2(l)}^0(t, y) C_{\text{Si}}^0(t, y) \right] dy,$$

722

$$(120) \quad P^1 = \frac{1}{U_g^0 C_g^0} \int_{y=0}^{y=z} \left[-\chi_1 C_C^0(t, y) \left(\frac{1}{2} - P_1(T(y)) \right) - \chi_2 \left(\frac{1}{2} - P_2(T(y)) \right)^+ + \chi_{-2} C_{\text{SiO}_2(l)}^0(t, y) C_{\text{Si}}^0(t, y) \right. \\ \left. - \chi_4 C_{\text{SiC}}^0(t, y) \left(\frac{1}{2} - P_4(T(y)) \right)^+ \right] dy,$$

724

$$725 \quad C_{\text{SiC}}^1 = \begin{cases} \chi_1 \int_{\tilde{t}=0}^{\tilde{t}=t} C_C^0(\tilde{t}, z) P^1(\tilde{t}, y) + C_C^1(\tilde{t}, z) \left(\frac{1}{2} - P_1 \right) d\tilde{t}, & P_4 \geq \frac{1}{2}, \\ e^{-\chi_4(\frac{1}{2}-P_4)t} \int_{\tilde{t}=0}^{\tilde{t}=t} e^{\chi_4(\frac{1}{2}-P_4)\tilde{t}} \left(\chi_1 C_C^0(\tilde{t}, z) P^1(\tilde{t}, y) + \chi_1 C_C^1(\tilde{t}, z) \left(\frac{1}{2} - P_1 \right) - \chi_4 C_{\text{SiC}}^0 P^1 \right) d\tilde{t}, & P_4 < \frac{1}{2}, \end{cases}$$

726

$$727 \quad (122) \quad C_{\text{Si}}^1 = \left(\alpha e^{-(T-T_m)t} + 1 - \alpha \right)^{\chi_{-2}} \int_{\tilde{t}=0}^{\tilde{t}=t} \left[\left(\alpha e^{-(T-T_m)\tilde{t}} + 1 - \alpha \right)^{-\chi_{-2}} \left(\chi_2 P^1(\tilde{t}, z) \mathbf{1}_{\{P_2 \leq \frac{1}{2}\}} \right. \right. \\ \left. \left. - \chi_{-2} C_{\text{SiO}_2(l)}^1(\tilde{t}, z) C_{\text{Si}}^0(\tilde{t}, z) + \chi_4 C_{\text{SiC}}^1(\tilde{t}, z) \left(\frac{1}{2} - P_4 \right)^+ + \chi_4 C_{\text{SiC}}^0(\tilde{t}, z) P^1(\tilde{t}, z) \mathbf{1}_{\{P_4 \leq \frac{1}{2}\}} \right) \right] d\tilde{t}.$$

Prescribed Temperature - Region Ia.

$$728 \quad (123) \quad C_C = 1 + \mathcal{O}(\epsilon^2),$$

729

$$730 \quad (124) \quad C_{\text{SiC}} = \epsilon \chi_1 \left(\frac{1}{2} - P_1 \right) \hat{t} + \mathcal{O}(\epsilon^2),$$

731

$$732 \quad (125) \quad C_{\text{SiO}_2(s)} = \alpha,$$

733

$$734 \quad (126) \quad C_{\text{SiO}_2(l)} = \epsilon \chi_2 \left(\frac{1}{2} - P_2 \right) \left(1 - e^{-\hat{t}} \right) + \mathcal{O}(\epsilon^2),$$

735

$$736 \quad (127) \quad C_{\text{Si}} = \epsilon \chi_2 \left(\frac{1}{2} - P_2 \right) \hat{t} + \mathcal{O}(\epsilon^2),$$

$$737 \quad (128) \quad U_g C_g = U_{g,IIa}^0 C_{g,IIa}^0(\hat{t}, z_m) + \epsilon \left(2 \int_{y=z_m}^{y=z} r_{5,Ia}^1(\hat{t}, y) - r_{2,Ia}^0(\hat{t}, y) dy + U_{g,IIa}^1 C_{g,IIa}^1(\hat{t}, z_m) \right) + \mathcal{O}(\epsilon^2),$$

$$738 \quad (129) \quad P = \frac{1}{2} - \epsilon \left(\frac{\int_{y=z_m}^{y=z} r_{1,Ia}^0(\hat{t}, y) + r_{2,Ia}^0(\hat{t}, y) dy}{U_{g,IIa}^1 C_{g,IIa}^1(\hat{t}, z_m)} - P_{IIa}^1(\hat{t}, z_m) \right) + \mathcal{O}(\epsilon^2),$$

739 where the functions $U_{g,IIa}^0 C_{g,IIa}^0$ and $U_{g,IIa}^1 C_{g,IIa}^1$ are the $\mathcal{O}(1)$ and $\mathcal{O}(\epsilon)$ terms in (102), P_{IIa}^1 is the $\mathcal{O}(\epsilon)$
740 term in (103), and the reaction rates are given by

$$741 \quad (130) \quad r_{1,Ia}^0(\hat{t}, z) = \chi_1 \left(\frac{1}{2} - P_1 \right), \quad r_{2,Ia}^0 = \chi_2 \left(\frac{1}{2} - P_2 \right), \quad r_{5,Ia}^1 = \chi_2 \left(\frac{1}{2} - P_2 \right) \left(1 - e^{-\hat{t}} \right).$$

742 **Prescribed Temperature - Region Ib.** In this region we have solutions

743 (131)
$$C_C = 1 - \epsilon \left(2\chi_1 \left(\frac{1}{2} - P_1 \right) + \chi_2 \left(\frac{1}{2} - P_2 \right) \right) t + \mathcal{O}(\epsilon^2),$$

744

745 (132)
$$C_{\text{SiO}_2(\text{s})} = \alpha,$$

746

747 (133)
$$C_{\text{SiO}_2(\text{l})} = \epsilon\chi_2 \left(\frac{1}{2} - P_2 \right) + \mathcal{O}(\epsilon^2),$$

748

749 (134)
$$U_g C_g U_{g,IIb}^0 C_{g,IIb}^0(t, z_m) + \epsilon U_{g,IIb}^1 C_{g,IIb}^1(t, z_m) + \mathcal{O}(\epsilon^2),$$

750 where $U_{g,IIb}^0 C_{g,IIb}^0$ and $U_{g,IIb}^1 C_{g,IIb}^1$ are the functions in region IIb, given in (110) and (119) respectively. We
751 also have

752 (135)
$$P \frac{1}{2} + \epsilon \left(P_{IIa}^1(t, z_m) - \frac{\int_{y=z_m}^{y=z} \chi_1 \left(\frac{1}{2} - P_1(T(y)) \right) + \chi_2 \left(\frac{1}{2} - P_2(T(y)) \right) dy}{U_{g,IIb}^0 C_{g,IIb}^0(t, z_m)} \right) + \mathcal{O}(\epsilon^2),$$

753

754 (136)
$$C_{\text{SiC}} \chi_1 \left(\frac{1}{2} - P_1 \right) t + \epsilon \left(\chi_1 \int_{\tilde{t}=0}^{\tilde{t}=t} P^1(\tilde{t}, z) d\tilde{t} - \left(\chi_1^2 \left(\frac{1}{2} - P_1 \right)^2 + \frac{\chi_1 \chi_2}{2} \left(\frac{1}{2} - P_1 \right) \left(\frac{1}{2} - P_2 \right) \right) t^2 \right) + \mathcal{O}(\epsilon^2),$$

755 where P^1 is the $\mathcal{O}(\epsilon)$ term in (135). We also have

756 (137)
$$C_{\text{Si}} \chi_2 \left(\frac{1}{2} - P_2 \right) t + \epsilon \left(\int_{\tilde{t}=0}^{\tilde{t}=t} \chi_2 P^1(\tilde{t}, z) d\tilde{t} - \frac{\chi_2 - 2\chi_2^2}{2} \left(\frac{1}{2} - P_2 \right)^2 t^2 \right) + \mathcal{O}(\epsilon^2).$$

757 **Full Model Asymptotics - Small diffusion limit.** Expanding variables in terms of K we have in
758 region A

759 (138)
$$T^A(z, t) = -1 + \omega F(z)t + \omega \sum_{n=1}^{\infty} K^n F^{(2n)}(z) \frac{t^{n+1}}{(n+1)!}, \quad C^A(z, t) = 0,$$

760 and that the position of the interface is given by

761 (139)
$$s(t) = F^{-1} \left(\frac{1}{\omega t} \right) - \frac{K}{2} \frac{F''(s_0(t))}{F'(s_0(t))} t + K^2 \left(\frac{F''(s_0(t))F'''(s_0(t))}{4(F'(s_0(t)))^2} - \frac{F^{IV}(s_0(t))}{6F'(s_0(t))} - \frac{(F''(s_0(t)))^3}{8(F'(s_0(t)))^3} \right) t^2 + \mathcal{O}(K^3).$$

762 In region B we have the leading order terms

763 (140)
$$C_0^B(z, t) = \frac{\exp \left(-\frac{2+b}{2\omega F(z)} + (b+1)t - \frac{b\omega F(z)}{2} t^2 \right)}{1 + \sqrt{\frac{\pi}{2b\omega F(z)}} \exp \left(\frac{1}{2b\omega F(z)} \right) \left[\operatorname{erf} \left(\frac{1}{\sqrt{2b\omega F(z)}} \right) + \operatorname{erf} \left(\frac{b\omega F(z)t - b - 1}{\sqrt{2b\omega F(z)}} \right) \right]},$$

764

765 (141)
$$T_0^B = \frac{1}{b}(C_0^B - 1) - 1 + \omega F(z)t.$$

766 The first order terms satisfy equations

767 (142)
$$b \frac{\partial T_1^B}{\partial t} - \frac{\partial C_1^B}{\partial t} = b \frac{\partial^2 T_0^B}{\partial z^2}, \quad \frac{\partial C_1}{\partial t} = -b(C_0^B T_1^B + C_1^B T_0^B),$$

768 with initial conditions

769 (143)
$$T_1^B + s_1(t) \frac{\partial T_0^B}{\partial z} = 0, \quad C_1^B + s_1(t) \frac{\partial C_0^B}{\partial z} = 0, \quad \text{on } t = \frac{1}{\omega F(z)}.$$

770 We can integrate the first equation in (142) to obtain

771 (144)
$$T_1^B = \frac{1}{b} C_1^B + \frac{F''(z)}{2\omega F(z)^2} + \int_{\tilde{t}=1/\omega F(z)}^{\tilde{t}=t} \frac{\partial^2 T_0^B}{\partial z^2}(z, \tilde{t}) d\tilde{t},$$

772 where the spatial function $F''(z)/2\omega F(z)^2$ has been determined using (143), (86), and (80), with $s_0(t) = z$
 773 and $t = 1/\omega F(z)$. Equation (144) can be substituted into the second equation in (142) to find

774 (145)
$$C_1^B(z, t) = \frac{1}{I(z, t)} \int_{\tilde{t}=1/\omega F(z)}^{\tilde{t}=t} I(z, \tilde{t}) \left[-\frac{bC_0^B(z, \tilde{t})F''(z)}{2\omega F(z)^2} - bC_0^B(z, \tilde{t}) \int_{u=1/\omega F(z)}^{u=\tilde{t}} \frac{\partial^2 T_0^B}{\partial z^2}(z, u) du \right] d\tilde{t} \\ + \frac{I(z, (\omega F(z))^{-1})}{I(z, t)} \frac{F''(z)}{2\omega F'(z)F(z)} \frac{\partial C_0^B}{\partial z} \Big|_{t=(\omega F(z))^{-1}},$$

775 where the integrating factor I is given by

776 (146)
$$I(z, t) = \exp \left(\int^{\tilde{t}=t} bT_0^B(z, \tilde{t}) + C_0^B(z, \tilde{t}) d\tilde{t} \right).$$

777 The solution in (145) can then be substituted into (144) to determine T_1^B .

778 **Acknowledgements.** This publication is based on work supported by the EPSRC Centre for Doctoral
 779 Training in Industrially Focused Mathematical Modelling (EP/L015803/1) in collaboration with Elkem. The
 780 authors thank Aasgeir Valderhaug, Rolf Birkeland, and Harald Wegge (all Elkem) for helpful discussions
 781 regarding this work. B. M. Sloman thanks Elkem for their financial support and the opportunity for on-site
 782 work during parts of this research.

783

REFERENCES

- 784 [1] J. T. ABRAHAMSON AND M. S. STRANO, *Analytical solution to coupled chemical reaction and thermally diffusing systems: applicability to self-propagating thermopower waves*, The Journal of Physical Chemistry Letters, 1 (2010), pp. 3514–3519.
 785
 786 [2] B. ANDRESEN, *Process model for carbothermic production of silicon metal*, PhD thesis, The Norwegian Institute of Technology, Trondheim, 1995.
 787 [3] E. S. ANTONIOU, J. K. BECHTOLD, AND M. MATALON, *A diffusional-thermal theory of near-stoichiometric premixed flames*, SIAM Journal on Applied Mathematics, 64 (2004), pp. 1434–1456.
 788 [4] H. M. BYRNE AND J. NORBURY, *Stable solutions for a catalytic converter*, SIAM Journal on Applied Mathematics, 54 (1994), pp. 789–813.
 789 [5] N. T. FADAI, C. P. PLEASE, AND R. A. VAN GORDER, *Asymptotic analysis of a multiphase drying model motivated by coffee bean roasting*, SIAM Journal on Applied Mathematics, (preprint) (2017).
 790 [6] N. D. FOWKES AND A. P. BASSOM, *Batch processing in a glass furnace*, The ANZIAM Journal, 57 (2015), pp. 175–188.
 791 [7] V. GUBERNOV, J. J. SHARPLES, H. S. SIDHU, A. C. MCINTOSH, AND J. BRINDLEY, *Properties of combustion waves in the model with competitive exo-and endothermic reactions*, Journal of Mathematical Chemistry, 50 (2012), pp. 2130–2140.
 792 [8] S. A. HALVORSEN, A. SCHEI, AND J. H. DOWNING, *A unidimensional dynamic model for the (ferro)silicon process*, in Electric Furnace Conference Proceedings, vol. 50, 1992.
 793 [9] D. R. LIDE, *CRC Handbook of Chemistry and Physics, 84 edn, 2004*, Section, 4:4–1.
 794 [10] D. R. LIDE, *CRC Handbook of Chemistry and Physics, 86 edn, 2005*, Section, 4:4–1.
 795 [11] B. F. LUND, *Rigorous simulation models for improved process operation*, PhD thesis, The Norwegian University of Science and Technology, Trondheim, 2005.
 796 [12] B. P. MARCHANT AND J. NORBURY, *Discontinuous travelling wave solutions for certain hyperbolic systems*, IMA journal of applied mathematics, 67 (2002), pp. 201–224.
 797 [13] J. NORBURY AND A. M. STUART, *A model for porous-medium combustion*, Quart. J. Mech. Appl. Math., 42 (1989), pp. 159–178.
 798 [14] H. OUTOKUMPU, *HSC Chemistry® for Windows, 4.0*, 1999.
 799 [15] P. PATNAIK, *Handbook of inorganic chemical compounds*, McGraw-Hill Professional, (2002), p. 1086.

810

- 811 [16] C. P. PLEASE, P. S. HAGAN, AND D. W. SCHWENDEMAN, *Light-off behavior of catalytic converters*, SIAM Journal on
812 Applied Mathematics, 54 (1994), pp. 72–92.
- 813 [17] C. P. PLEASE, F. LIU, AND D. L. S. McELWAIN, *Condensed phase combustion travelling waves with sequential exothermic or endothermic reactions*, Combustion Theory and Modelling, 7 (2003), pp. 129–143.
- 814 [18] A. SCHEI, J. K. TUSET, AND H. TVEIT, *Production of high silicon alloys*, Tapir, Trondheim, Norway, 1998.
- 815 [19] L. A. SEGEL AND M. SLEMROD, *The quasi-steady-state assumption: a case study in perturbation*, SIAM Rev., 31 (1989),
816 pp. 446–477.
- 817 [20] J. J. SHARPLES, H. S. SIDHU, A. C. McINTOSH, J. BRINDLEY, AND V. GUBERNOV, *Analysis of combustion waves arising in the presence of a competitive endothermic reaction*, IMA Journal of Applied Mathematics, 77 (2012),
818 pp. 18–31.
- 819 [21] B. M. SLOMAN, C. P. PLEASE, R. A. VAN GORDER, A. M. VALDERHAUG, R. G. BIRKELAND, AND H. WEGGE, *A heat and mass transfer model of a silicon pilot furnace*, Metallurgical and Materials Transactions B, 48 (2017),
820 pp. 2664–2676.
- 821 [22] A. M. VALDERHAUG, *Modelling and control of submerged-arc ferrosilicon furnaces*, PhD thesis, The Norwegian Institute
822 of Technology, Trondheim, 1992.
- 823 [23] S. O. WASBØ AND A. HAMMERVOLD, *SiMod - a Silicon Furnace Process Model*. Personal Communication, 2014.
- 824 [24] W. WEE, H. SIDHU, J. SHARPLES, I. TOWERS, AND V. GUBERNOV, *Properties of reaction fronts in a non-adiabatic two*
825 *stage exothermic-endothermic competitive reaction scheme*, ANZIAM Journal, 54 (2013), pp. 646–663.
- 826
827
828